

154  
1987  
52454  
c. 3

Pulsating flow through models of compliant stenoses

by

Nikolaos Stergiopoulos

A Thesis Submitted to the  
Graduate Faculty in Partial Fulfillment of the  
Requirements for the Degree of  
MASTER OF SCIENCE

Interdepartmental Program: Biomedical Engineering  
Major: Biomedical Engineering

Signatures have been redacted for privacy

Iowa State University  
Ames, Iowa

1987

## TABLE OF CONTENTS

	PAGE
INTRODUCTION . . . . .	1
LITERATURE REVIEW . . . . .	6
Physiological Considerations . . . . .	6
Rheological characteristics of blood . . . . .	6
Properties of the arterial wall . . . . .	7
Flow in the arterial system . . . . .	8
Reynolds number . . . . .	9
Alpha parameter . . . . .	9
Pulsatile Flow Studies . . . . .	10
Collapsible Tube Studies . . . . .	12
Stenosis Studies . . . . .	15
Stenosis geometry . . . . .	16
Rigid stenoses . . . . .	18
Analytical studies . . . . .	19
Experimental studies . . . . .	19
Dimensional analysis . . . . .	20
Pressure-flow relationship . . . . .	21
Arterial stenosis . . . . .	25
Effect of vasomotor tone . . . . .	25
Vasoconstriction . . . . .	25
Vasodilation . . . . .	27
Effect of intraluminal pressure . . . . .	28
Models of compliant arterial stenosis . . . . .	28
MATHEMATICAL MODEL . . . . .	33
Rigid Stenosis Models . . . . .	33
Effects of Compliance - Pressure-Area Relation . . . . .	35
The Mathematical Model . . . . .	38
MATERIALS AND PROCEDURES . . . . .	40
Materials . . . . .	40
Stenosis characteristics . . . . .	42
Collapsible tube properties . . . . .	42
Fluid properties . . . . .	43
Experimental Set-Up . . . . .	43
Flow system . . . . .	43
Data aquisition system . . . . .	46
Sensing devices . . . . .	46
Amplifier . . . . .	46
Digitizer and micro-computer . . . . .	46
Procedures . . . . .	47
Pulsatile flow tests . . . . .	47
Stenosis preparation . . . . .	47
Equipment calibration . . . . .	48
Pulsatile flow tests . . . . .	48
Data Processing . . . . .	49

Signal averaging and filtering . . . . .	50
Pressure drop calculation . . . . .	50
Parameter estimation - Statistical analysis . . . . .	51
Estimation of $p^*$ . . . . .	51
Estimation of $\beta$ and $C/A_0$ . . . . .	52
Evaluation of the Experimental Set-Up . . . . .	53
RESULTS AND DISCUSSION . . . . .	56
Parameter Estimation . . . . .	56
Estimation of $\beta$ and $C/A_0$ . . . . .	56
Theoretical vs Experimental Data . . . . .	58
Significance of the Compliance . . . . .	59
Interdependence of the Parameters . . . . .	79
Dependence of $\beta$ on $p^*$ . . . . .	79
Dependence of effective compliance on $p^*$ . . . . .	79
Stenosis in Collapsing Mode . . . . .	80
SUMMARY AND CONCLUSIONS . . . . .	90
BIBLIOGRAPHY . . . . .	96
ACKNOWLEDGMENTS . . . . .	100
APPENDIX . . . . .	101
Method . . . . .	101
The Numerical Technique . . . . .	103

## LIST OF TABLES

	PAGE
TABLE 1. Model and flow parameters for the non-collapsing pulsatile flow tests . . . . .	58
TABLE 2. Dependence of $\beta$ on $p^*$ ( $4.5 < a < 4.8$ ) . . . . .	79
TABLE 3. Dependence of $C/A_0$ on $p^*$ ( $4.5 < a < 4.8$ ) . . . . .	80

## LIST OF FIGURES

	PAGE
FIGURE 1. Typical model for stenosed artery. From Dubill, 1986 . . . . .	4
FIGURE 2. Cross sections for rigid and compliant stenoses. From Dubill, 1986 . . . . .	4
FIGURE 3. Starling Resistor Device. From Conrad, 1969 . . . . .	13
FIGURE 4. Cross-section of an eccentric stenosis. From Brown et al., 1984 . . . . .	17
FIGURE 5. Human coronary stenoses. From Freudenburg and Lichtlen, 1981 . . . . .	18
FIGURE 6. General stenosis geometry. From Young, 1979 . . . . .	21
FIGURE 7. Flow pulse waveform. From Young, 1979 . . . . .	22
FIGURE 8. Pressure-flow curves for 85% stenosis, at different external pressures. The dotted line denotes stenosis in collapsed state. From Dubill, 1986 . . . . .	32
FIGURE 9. Photograph of the stenosed segment . . . . .	41
FIGURE 10. Schematic representation of the stenosed segment . . . . .	41
FIGURE 11. Stenosis characteristics . . . . .	42
FIGURE 12. Photograph of the flow system . . . . .	44
FIGURE 13. Schematic diagram of the flow system . . . . .	45
FIGURE 14. Theoretical vs measured pressure drop . . . . .	55
FIGURE 15. Pressure drop waveforms for the 74% stenosis ( $a=4.7$ ) . . . . .	60

FIGURE 16.	Pressure drop waveforms for the 74% stenosis ( $a=5.9$ ) . . . . .	61
FIGURE 17.	Pressure drop waveforms for the 74% stenosis ( $a=6.4$ ) . . . . .	62
FIGURE 18.	Pressure drop waveforms for the 82% stenosis ( $a=4.7$ ) . . . . .	63
FIGURE 19.	Pressure drop waveforms for the 82% stenosis ( $a=5.9$ ) . . . . .	64
FIGURE 20.	Pressure drop waveforms for the 82% stenosis ( $a=6.4$ ) . . . . .	65
FIGURE 21.	Pressure drop waveforms for the 88% stenosis ( $a=4.5$ ) . . . . .	66
FIGURE 22.	Pressure drop waveforms for the 88% stenosis ( $a=5.9$ ) . . . . .	67
FIGURE 23.	Pressure drop waveforms for the 88% stenosis ( $a=6.4$ ) . . . . .	68
FIGURE 24.	Flow waveform for the 74% stenosis ( $a=4.8$ ) . . . . .	69
FIGURE 25.	Flow waveform for the 82% stenosis ( $a=4.7$ ) . . . . .	70
FIGURE 26.	Flow waveform for the 88% stenosis ( $a=4.5$ ) . . . . .	71
FIGURE 27.	Variation in stenosis lumen area for the 74% stenosis ( $a=4.8$ ) . . . . .	72
FIGURE 28.	Variation in stenosis lumen area for the 82% stenosis ( $a=4.7$ ) . . . . .	73
FIGURE 29.	Variation in stenosis lumen area for the 88% stenosis ( $a=4.5$ ) . . . . .	74
FIGURE 30.	Compliant vs rigid 74% stenosis ( $a=4.8$ ) . . . . .	76
FIGURE 31.	Compliant vs rigid 82% stenosis ( $a=4.7$ ) . . . . .	77
FIGURE 32.	Compliant vs rigid 88% stenosis ( $a=4.5$ ) . . . . .	78
FIGURE 33.	Pressure and flow waveforms for the 74% stenosis in collapsed mode ( $a=4.8$ ) . . . . .	82

- FIGURE 34. Proximal and distal pressure waveforms for the 74% stenosis in collapsed mode ( $a=4.8$ ) . . . 83
- FIGURE 35. Pressure and flow waveforms for the 82% stenosis in collapsed mode ( $a=4.7$ ) . . . . . 84
- FIGURE 36. Proximal and distal pressure waveforms for the 82% stenosis in collapsed mode ( $a=4.7$ ) . . . 85
- FIGURE 37. Pressure and flow waveforms for the 88% stenosis in collapsed mode ( $a=4.5$ ) . . . . . 86
- FIGURE 38. Proximal and distal pressure waveforms for the 88% stenosis in collapsed mode ( $a=4.5$ ) . . . 87

## INTRODUCTION

Arterial stenosis, which refers to a constricted or a narrowed segment of an artery, is a frequent result of arterial disease. In most of the cases arterial stenosis can be attributed to the deposition of atherosclerotic plaque on the arterial wall. As these plaque develop they project into the lumen of the artery, causing a localized narrowing for the passage of blood through the vessel. With the development of a stenosis the flow pattern distal to the stenosis is altered significantly. When the stenosis is severe enough, the flow alteration can be accompanied with turbulence, separation phenomena, and pressure loss across the stenosis.

The physiological significance of the aforementioned stenosis induced alterations is quite striking. It has been shown experimentally that the changing of the flow characteristics in the vicinity of stenosis triggers certain biological mechanisms that may lead to cell damage, abnormal cell growth and further development of the stenosis. On the other hand, pressure loss across the stenosis can reduce the blood flow to the peripheral beds that the artery supplies. When the stenosed artery is one of the coronary arteries that supplies the myocardium, reduced blood flow can result in severe chest pain or even myocardial infarction, the

leading cause of death in the United States. When the blockage occurs in one of the carotid arteries, reduced blood flow to the brain can cause stroke, the third leading cause of death in the United States. Thus, it is not surprising that during the last two decades, much effort has been put into studying the fluid mechanics of arterial stenoses. In general, the fluid mechanics problems related to the arterial stenoses can be grouped into three broad categories (Young, 1979):

1. Effect of the stenosis on regional blood flow to peripheral vascular beds
2. Localized hydrodynamic effects such as pressure distribution along the stenosis, wall shearing stress distribution, velocity distribution, separation phenomena and turbulence
3. Methods for detection and clinical evaluation of stenoses.

Due to the complexity of the phenomenon, most of the stenosis studies that were done in the past were experimental, although investigations involving numerical approaches and computer modeling have become of more recent interest. The experimental studies can either be in vivo or in vitro studies. In vivo experiments involve naturally occurring or artificially induced stenoses in real arteries,

whereas in in vitro experiments a hydraulic model is employed to simulate the arterial flow. The in vitro experiments have proven to be extremely helpful for two reasons: first, because the complex system that exists in the body is greatly simplified, thus allowing better control of the various parameters that enter the system, and second, because measurements can be designed and performed in a more accurate and reliable way. Hydraulic models of arterial stenoses may vary considerably with respect to the specific characteristics of the stenosed artery they resemble or the degree of simplification. A typical hydraulic model is drawn in Fig. 1. The stenosed artery is modeled as a straight tube with some kind of constriction and the downstream resistances are all lumped together into a single distal resistance. Two types of stenoses have been used in model stenoses studies. Rigid stenoses, in which the geometry of the stenoses remains unchanged, and compliant stenoses that are partially circumscribed by a normal, compliant, wall segment capable of undergoing a change in geometry, as shown in Fig. 2.

Undoubtedly, the easiest case to consider is a model with rigid stenosis and perfused with steady flow. Such models have been extensively studied in the past and have provided a great insight in the fluid mechanics of arterial

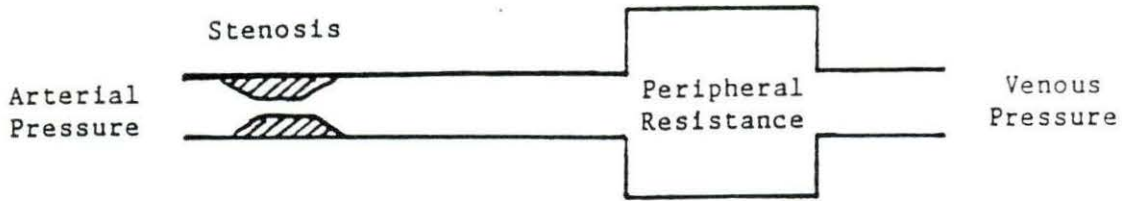


FIGURE 1. Typical model for stenosed artery. From Dubill, 1986

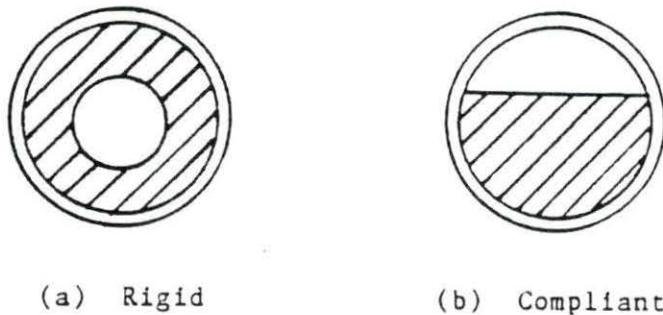


FIGURE 2. Cross sections for rigid and compliant stenoses. From Dubill, 1986

stenoses. It is a fact, however, that blood flow through the arteries is highly pulsatile. Moreover, it has been suggested that the majority of the human stenoses are compliant to some extent (Brown et al., 1984). Compliant stenoses are of particular clinical interest because they are associated with a potential flow limiting situation due to a collapse of the artery. Although this extreme case attracts most of the attention, the dynamic nature of the

compliant stenosis is not limited there. The fact that compliant stenoses behave dynamically when they are not in a collapsed mode has received little attention so far. The purpose of the present study was to investigate the relationship between pulsatile flow and a compliant stenosis, and to give some insight into the mechanics of this complicated phenomenon.

More specifically, the objectives of this thesis were:

- To examine the effect of the compliant stenosis on the flow characteristics, particularly in a non-collapsed mode.
- To develop a theoretical model for pulsatile flow through a compliant stenosis and to identify the various parameters that enter the problem.
- To assess the validity of using steady flow models for compliant stenoses.
- To evaluate the applicability of the experimental set-up for general pulsatile flow studies involving compliant stenoses.

## LITERATURE REVIEW

Before preceding to the formulation of the mathematical model and the description of the experimental procedures, some physiological characteristics important in designing and evaluating the model are considered. In addition, previous relevant studies on pulsatile and stenotic flow that provide valuable background to the present study, are reviewed in the following paragraphs.

## Physiological Considerations

The physiological characteristics considered were the rheological properties of blood, the mechanical properties of the arterial wall, and the mechanics of flow in the arterial system.

Rheological characteristics of blood

Blood is a non-Newtonian fluid. In its simplest description, blood is a suspension of red blood cells (erythrocytes) in plasma. Although plasma in general exhibits Newtonian behavior, blood as a whole shows two kinds of viscous abnormalities. First, at low shear rates,  $\dot{\gamma}$  ( $\dot{\gamma} < 100$  1/s), the apparent viscosity increases exponentially, and second, the apparent viscosity depends on the size of the vessel. In small vessels (diameter < 1mm),

the viscosity drops significantly, reaching its minimum value in vessels of approximately  $100\mu$  in diameter. This phenomenon is known as the Farheous-Lindquist effect. Blood viscosity depends also on the hematocrit level. Hematocrit is a measure of the relative volume that the red blood cells occupy, and can vary from species to species or in abnormal situations such as anemia. Fortunately, at shear rates above about  $100 \text{ l/s}$ , blood viscosity approaches an asymptotic value and can be assumed to be practically constant. Shear rates higher than  $100 \text{ l/s}$  are typical in large arteries (McDonald, 1974).

Typical values for the viscosity of the human and the canine range from  $3\text{-}4 \times 10^{-3} \text{ Ns/m}^2$  for shear rates greater than  $100 \text{ s}^{-1}$  and normal body temperature (Milnor, 1982). Literature values for the blood density range from  $1050$  to  $1060 \text{ kg/m}^3$ .

#### Properties of the arterial wall

Because of its non-homogeneous, multi-layer structure, the arterial wall exhibits anisotropic, non-linear, viscoelastic behavior. Thus, the modulus of elasticity,  $E$ , rather than being constant at a particular arterial segment, depends on both the direction and the load (stress). Viscoelasticity introduces some extra difficulties, since additional variables like time and frequency should be

considered when studying the elastic performance of the arterial wall.

For analysis purposes, a single value for the modulus of elasticity, referred to as the incremental modulus of elasticity,  $E_{inc}$ , is often used. The value of  $E_{inc}$  is valid for a specific artery or arterial segment and over a defined range of applied stress, where linearity on the stress-strain relationship is assumed. Typical values for  $E_{inc}$  for various arteries and veins are given by Caro et al. (1978).

The elastic properties of the arterial wall are important determinants of certain circulatory phenomena, such as wave propagation and the distension of the arterial wall. Both phenomena have received considerable attention, and several simplified theories leading to applicable equations for the wave transmission and the pressure-area relations are cited in the literature. A complete review is given by Milnor (1982).

### Flow in the arterial system

The interaction of the pulsatile flow and the complex geometry and properties of arterial tree have a unique effect on the blood flow characteristics. As the blood flows from aorta to the capillaries, flow is altered continuously, going from an almost turbulent flow in the aorta to a slow flow in which viscous effects are strong in

the arterioles, and from highly pulsatile in the large arteries to 'quasi-steady' at the arteriolar level. This diversity in the flow patterns throughout the arterial system, reflects on a surprisingly wide spectrum of Reynolds numbers and alpha parameters found in the human circulation.

These parameters are described as follows:

Reynolds number      The Reynolds number is a dimensionless parameter defined as

$$Re = \frac{\rho DV}{\mu}$$

where:

$\rho$  = density of blood

D = internal diameter of the vessel

$\mu$  = viscosity of blood

V = velocity of blood flow

The Reynolds number expresses the relative importance between the inertial and viscous forces. Under steady flow conditions, the Reynolds number serves also as a criterion to determine the transition from laminar flow to turbulent flow. Typical values for the mean Reynolds number found in the literature range from about 100 in small arteries to 12000 in the aorta.

Alpha parameter      The alpha parameter,  $a$ , sometimes called the Womersley or frequency parameter, is one of the

governing parameters for oscillating flows, and can be defined as:

$$a = R \sqrt{\omega/\nu}$$

where:

R = the vessel radius

$\omega$  = the angular frequency corresponding to pulse rate

$\nu$  = the kinematic viscosity of the fluid

From the fluid mechanics standpoint,  $a$  can be viewed as the ratio of the local acceleration forces to viscous forces. High  $a$  values ( $a \gg 1$ ) indicate that the flow is highly pulsatile and the inertial forces are predominate. At low  $a$  values ( $a < 1$ ), the type of flow is 'quasi-steady'; the viscous forces dominate and the inertial effects can be neglected. The  $a$ -values for the human arteries range from as low as 1 for the small arteries to about 17 in aorta (McDonald, 1974).

#### Pulsatile Flow Studies

It is well-established that blood flow is highly pulsatile in all systemic arteries. Even in small arteries like the saphenous artery, the alpha parameter has a value of approximately one, showing some pulsatility in the flow (McDonald, 1974). Thus, for a complete analysis of arterial flows inertial effects cannot be neglected.

The problem of laminar oscillating flow in a straight rigid tube, which is the simplest approach in modeling arterial flows, has been studied in the past and solutions are well-known. Several investigators obtained analytical solutions to the problem (Schonfeld, 1949; Uchida, 1956; Womersley, 1955a). In each of the aforementioned studies, the pressure gradient waveform was resolved into its harmonics, and an ordinary differential equation was derived as a basic relation for each of the harmonics. The solution to the differential equation was expressed in terms of Bessel functions. Womersley expanded his work to more realistic models, developing a consistent treatment for elastic tubes (1955b) and viscoelastic tubes (1957).

Another approach to the same problem was presented by Fry (1959). Starting from the same differential equation used by Womersley, Fry arrived at the approximate relationship between pressure gradient and flow

$$\frac{\Delta p}{\Delta x} = RQ + L \frac{dQ}{dt} \quad (1)$$

The above equation was solved by means of an electrical analog. The idea behind it was that once the empirical coefficients R and L were determined, their values could be used to give the flow waveform, when the pressure gradient was the measured quantity. Although semiempirical, Fry's

solution checks out well with the more precise Womersley's solution for physiological flows (Greenfield and Fry, 1965).

Today, the development of the high-speed digital computers enables scientists and engineers to apply numerical solutions to many of the traditional fluid mechanics problems. Such a numerical solution to the Womersley problem is presented in the Appendix, and results of this solution are used in the present study to validate the experimental apparatus.

### Collapsible Tube Studies

A phenomenon of major medical interest closely associated with blood flow dynamics, is the phenomenon of arterial collapse. When the transmural pressure that keeps the arteries distended falls below a critical point, arteries can collapse. Arterial collapse causes severe changes in the vessel geometry reducing their lumen markedly and leading to flow limiting situations.

Many investigators have studied the characteristics of flow through collapsible tubes using a simple device, called the Starling resistor. As shown in Fig. 3, the Starling resistor is simply a thin-walled elastic tube inside a pressure chamber. The important quantities that define the behavior of the system are the volume rate of flow,  $Q$ , the

inlet pressure,  $P_1$ , the outlet pressure,  $P_2$  and the external pressure,  $P_e$ .

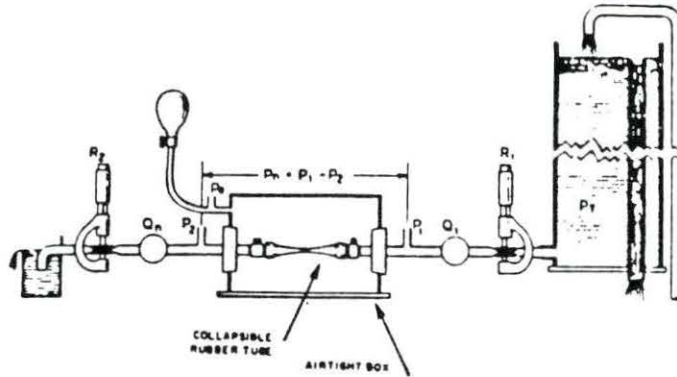


FIGURE 3. Starling Resistor Device. From Conrad, 1969

Early work by Rodbard and Saiki (1953) and Rodbard (1955) revealed some of the important aspects of flow in collapsible tubes. Rodbard dealt mainly with the paradox of increased flow when a resistance was added at the outlet of the system. Rodbard also pointed out that a partially collapsed tube results in the production of noisy flutter and high energy losses along the tube. Conrad (1969) performed systematic studies on collapsible tubes, using the Starling resistor device. From his experiments Conrad concluded that three distinct flow states exist, characterized by the relative value of the transmural

pressure to a critical transmural pressure,  $P_{Cr}$ . When the transmural pressure ( $P-P_e$ ) is greater than  $P_{Cr}$ , then the tube is wide open and Poiseuille's law applies. When the transmural pressure ( $P-P_e$ ) equals  $P_{Cr}$ , then the tube is partially collapsed and the relationship between flow and pressure is non-linear. When ( $P-P_e$ ) is less than  $P_{Cr}$ , the tube is fully collapsed and the  $P_1-P_2$  versus  $Q$  relationship appeared to be linear but with steeper slope from the linear case. Using Conrad's data, Brower and Noordergraaf (1973) developed theoretical models proposing that the pressure differences ( $P_1-P_2$ ) and ( $P_2-P_e$ ) were the significant variables. Earlier, Lopez-Muniz et al. (1968) had suggested that for the collapsed state  $Q$  is proportional to  $P_1-P_e$ , and changes in  $P_2$  have no influence on the flow rate,  $Q$ .

Several attempts have been made to analyze the physical behavior of the Starling resistor device by means of mathematical models. These studies can be grouped into two distinct categories according to the mechanism of flow limitation each group proposes.

The first mechanism is called the "inertial mode of flow limitation", (Elliott and Dawson, 1978; Shapiro, 1977). The independence between upstream and downstream pressure in a choked (collapsed) segment, is attributed to the development of local pulse-wave conditions. An important

variable in the analysis was the speed of pressure waves in the tube. Griffiths suggested that flow in the uncollapsed portion of the tube is subsonic whereas in the collapsed portion it is supersonic, building thus a transonic barrier for the upstream propagation of the pressure waves.

The second mechanism is called the "frictional mode of limitation", (Rubinow and Keller, 1972; Fry et al., 1980). According to Fry et al., "the principle of the mechanism is based on the fact that changes in the outlet pressure, alter the pressure distribution in the downstream segment of the collapsible tube, causing compensatory changes in the flow resistance of this segment in a direction such that flow is maintained virtually constant." Rubinow and Keller analyzed the mechanism both experimentally and mathematically and found good agreement between experimental and theoretical values, in their studies on the human iliac artery. For these basic studies on flow in collapsible tubes there are no stenoses present.

### Stenosis Studies

Arterial stenosis has a complex effect on the dynamics of blood flow. Some of the important hemodynamic features associated with the presence of stenosis in the arterial system are greater resistance to flow, flow separation,

turbulence, post-stenotic dilatation and possible arterial collapse. Recognizing the complexity of the phenomenon, several investigators pursued studies on in-vivo and in-vitro models of stenoses. These studies provided insight into the hemodynamics of the arterial stenosis, and some of their findings regarding stenosis geometry, and the fluid mechanics of rigid and compliant stenosis are discussed in the following sections.

### Stenosis geometry

Stenoses may differ markedly in their morphological characteristics, such as shape, length and severity. In addition, stenoses may contain a part of normal arterial wall as opposed to "fixed" or "rigid" stenoses, where the calcified atheroma covers the whole circumference of the stenotic lesion. Figure 4 shows a coronary stenosis with a normal wall segment (dashed line). Because of their configuration, the term "eccentric" is used to characterize this type of stenosis. Figure 5 shows some idealized drawings of concentric and eccentric stenoses. Although both types exist in the human circulation, post mortem studies reported in the literature suggest that the majority of human (coronary) stenoses are compliant (Freudenburg and Lichtlen, 1981; Maseri et al., 1978).



FIGURE 4. Cross-section of an eccentric stenosis. From Brown et al., 1984

Stenosis severity is usually expressed in terms of percent area reduction denoted as percent stenosis defined as

$$\text{Percent stenosis} = (1 - A_1/A_0) \times 100$$

where:

$A_1$  = free cross-sectional area

$A_0$  = unobstructed lumen area

Several other pertinent geometric characteristics, such as shape, divergence-convergence angle and smoothness are needed to define the geometry of the stenosis. However, for simplicity, most investigators do not take these factors

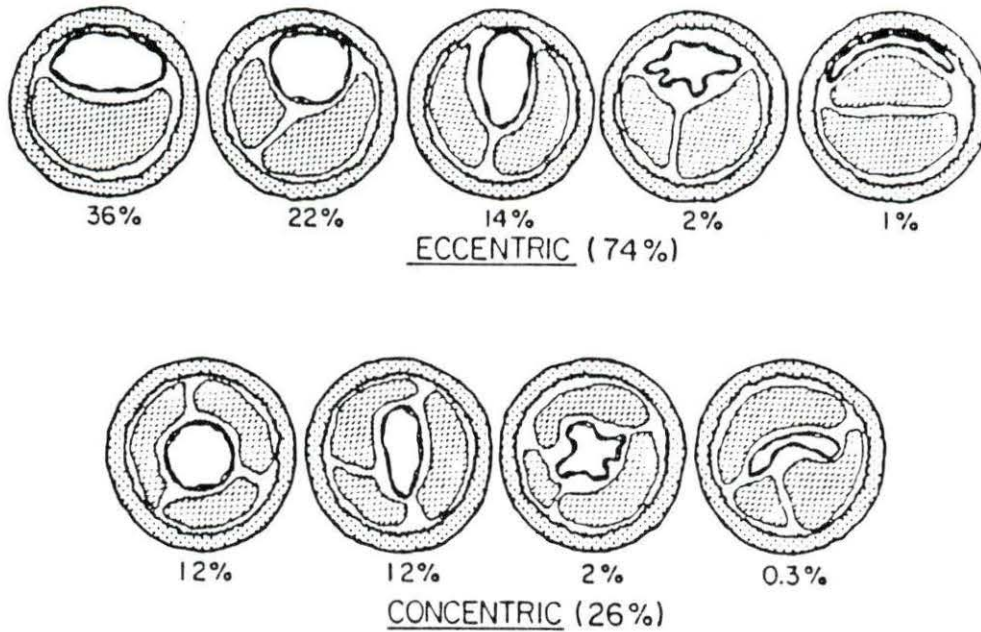


FIGURE 5. Human coronary stenoses. From Freudenburg and Lichtlen, 1981

into account. In fact, Seeley and Young (1976) studying the effect of geometry on the fluid mechanics of the stenosis, showed that equations developed for regular-shaped models could be used to approximately describe flow in irregular models.

#### Rigid stenoses

Although it is generally recognized that in the circulation stenoses often behave in dynamic fashion (Brown et al., 1984; Santamore et al., 1980), rigid stenoses

studies provide valuable background on various aspects of the fluid mechanics of the arterial stenosis.

Analytical studies      Attempts to find analytical solutions for the flow through stenoses were limited to simple, axisymmetric geometries and to non-turbulent flows. Young (1968) performed an analysis for a mild, axisymmetric configuration, to obtain an approximate solution, based on the elimination of the convective acceleration terms of the Navier-Stokes equations. Forrester and Young (1970) extended the same analysis to account for the occurrence of flow separation. Following a different approach which utilizes both integral-momentum and integral-energy equations, Morgan and Young (1974), arrived at a solution that holds for either mild or more severe stenoses, on the presumption that flow remains still in the laminar region. Lee and Fung (1970) used a numerical scheme to solve the problem for mild and severe stenoses, including the presence of flow separation.

Experimental studies      The applicability of analytical or numerical methods, to the general case of flow through stenoses, is rather restricted by the presence of turbulence and the infinite variety of possible stenosis geometries. Thus, a great deal of experimental work has been done to study the various aspects of stenotic flow.

Important aspects of the experimental studies were the dimensional analysis, which reveals the various factors that influence the fluid mechanics of the stenosis, and the specific pressure-flow relationship

Dimensional analysis One of the most important hemodynamic quantities associated with the arterial stenosis, is the pressure drop across it,  $\Delta P$ . The effect of pressure drop can be dramatic. If  $\Delta P$  is great enough, pressure distal to stenosis can be reduced to such a degree that blood flow to the peripheral beds, despite the local compensatory mechanisms the body applies (i.e., vasodilation), is greatly reduced. Therefore, a good understanding of the factors that influence the pressure drop, as well as the knowledge of the relationship between flow and pressure drop, is considered essential.

Young (1979) performed a dimensional analysis for the pulsatile flow case and a generalized geometry. Figure 6 shows the geometry of the stenosis and the parameters needed to define it. The flow waveform parameters are shown in Fig. 7. As a result, the following equation for the pressure drop was obtained:

$$\frac{\Delta p}{\rho U^2} = f\left(\frac{L}{D}, \frac{A_1}{A_0}, \frac{\lambda_i}{D}, \frac{DU_p}{\nu}, \frac{U_s}{U_p}, \frac{\tau_1}{\tau}, \frac{t}{\tau}, \frac{D}{2} \sqrt{\frac{2\pi}{\tau\nu}}\right) \quad (2)$$

where:

$\Delta p$  = pressure drop across the stenosis

$U$  = mean fluid velocity

$U_p$  = peak fluid velocity

$\tau$  = period of the pulse

$D$  = diameter of the tube

$\lambda_i$  = characteristic lengths that define the stenosis geometry

$A_0$  = cross-sectional area of the unobstructed tube

$A_1$  = minimum free cross-sectional area of the stenosis

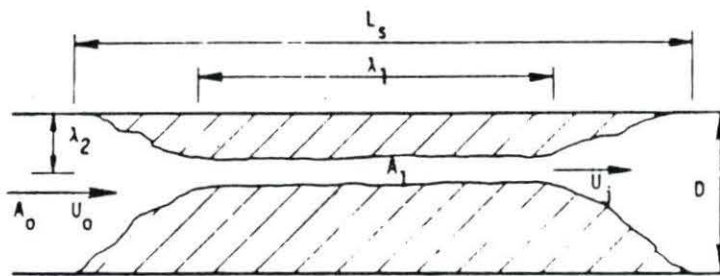


FIGURE 6. General stenosis geometry. From Young, 1979

#### Pressure-flow relationship Young and Tsai

(1973a and 1973b) performed extensive studies on the flow characteristics of model stenoses. They found that in the general case of unsteady flow, the pressure drop,  $\Delta P$ , can be estimated from the equation

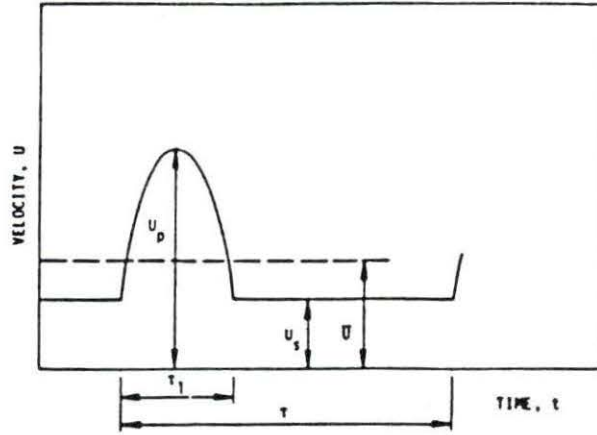


FIGURE 7. Flow pulse waveform. From Young, 1979

$$\Delta p = \frac{K_V \mu}{d} U + \frac{K_t}{2} \left[ \frac{A_0}{A_1} - 1 \right]^2 \rho |U| U + K_U \rho L \frac{dU}{dt} \quad (3)$$

where:

$A_0$  = cross-sectional area of unobstructed tube

$A_1$  = minimum free cross-sectional area of the stenosis

$K_V$ ,  $K_t$ , and  $K_U$  = experimentally determined coefficients

The first term on the right of Eq. 3 represents the pressure drop due to viscous effects. The second term, is associated with the divergence and convergence of the flow in the stenosis and accounts for the turbulent losses. The third term, present only in pulsatile flow, accounts for the pressure gradient needed to accelerate the fluid. Viscous effects dominate at low Reynolds numbers, whereas the turbulent effects will dominate at moderate to high Reynolds numbers, usually found in the arterial flow.

The empirical coefficients  $K_v$ ,  $K_t$ , and  $K_u$  in general depend on the geometry of the stenosis and the alpha parameter. Seeley and Young (1976) studied the effects of geometry on steady flow through blunt plugs and found that  $K_v$  depends strongly on the geometry and can be approximated by the equation

$$K_v = 32 \left( \frac{L_a}{d} \right) \left( \frac{A_0}{A_1} \right)^2 \quad (4)$$

where

$$L_a = 0.83L_s + 1.46d_1$$

and  $L_s$  is the stenosis length and  $L_a$  represents an equivalent stenosis length that accounts for the entrance and exit effects. In the same paper, Seeley and Young suggested that  $K_t$  is not strongly dependent on geometry, and has an approximately constant value of 1.52. The coefficient  $K_u$  is also assumed to be fairly constant, with an approximate value of 1.2 (Young and Tsai, 1973b).

A summary of the important conclusions coming from the evaluation of Eq. 3 was given by Young (1979):

1. Although  $\Delta P$  is influenced by several factors such as geometry, viscosity and density of blood, velocity and flow waveform, in the physiological

range the most important factors are the area ratio,  $A_1/A_0$  and the velocity.

2. The pressure drop varies non-linearly with the velocity, thus, the effective stenosis resistance is velocity dependent.
3. Due to its non-linear effect, the ratio  $A_1/A_0$  (usually expressed in terms of percent stenosis) becomes a very important factor when a critical point is reached. Beyond this point, small changes in percent stenosis have a dramatic effect on the pressure drop. This critical percent stenosis is lower at elevated flow rates.
4. For moderate to severe stenoses where the viscous effects are small, variations in viscosity and stenosis length are considered insignificant.
5. For moderate and severe stenoses the acceleration effects are negligible.

Equation 3 was verified through in-vivo experiments by Young et al. (1975). Pressure drop across artificially induced stenosis in the femoral artery of dogs was compared with those predicted from Eq. 3. Results showed a reasonable agreement and supported the applicability of the equation for actual arterial flow.

### Arterial stenosis

A common observation of many investigators concerned with the hemodynamics of coronary and carotid arteries was that, rather than being fixed, arteries could alter their severity as a response to various stimuli. Such a behavior is in contrast with the traditional concept of rigid stenoses and suggests that stenoses behave in a dynamic fashion. Indeed, it has been reported (Maseri et al., 1978) that diseased stenotic regions often contain a segment of normal arterial wall, able to change geometry under the influence of vasomotor tone and intraluminal pressure.

Effect of vasomotor tone Vasomotor tone refers to the contractile state of the smooth muscle, present in all systemic arteries. Arterial smooth muscle, often referred to as the "active element" of the arterial wall, can contract (vasoconstriction) or relax (vasodilation) in response to various pharmacological agents, called vasoconstrictor and vasodilator drugs, respectively.

Vasoconstriction The effect of vasoconstriction on compliant stenoses becomes a very important determinant of the role of coronary artery spasm. Coronary artery spasm refers to an inappropriate constriction of the large coronary arteries, with the mechanism causing it yet to be made clear (Santamore, 1986).

Increasing evidence that episodes of angina pectoris (chest pain) could be caused by arterial spasm superimposed on coronary artery stenoses has drawn the attention of many investigators over the last few years.

Santamore et al. (1980) studied the effects of arterial vasoconstriction on stenotic hemodynamics, in in-vitro coronary artery preparations. The in-vitro preparation was chosen to eliminate uncontrolled neural, humoral, and systemic effects. Two types of stenoses were used; one of fixed geometry, created by tightening an external snare around the vessel, and another, created by inflating an intraluminal balloon catheter, thus allowing vasoconstriction to occur. Vasoconstriction was induced and the resistance to flow was measured. Vasoconstriction itself without the presence of stenosis, had no significant effect on flow. Similarly, with the presence of stenosis produced with the external snare, vasoconstriction had a little additional effect on the flow reduction. With the stenosis produced by the intraluminal balloon catheter, arterial vasoconstriction caused a dramatic increase in the stenotic resistance.

Anticipating the possible mechanisms of the phenomenon, Santamore et al. indicated that for a critical stenosis, a small reduction in diameter (caused by vasoconstriction),

could significantly increase the severity or even totally occlude the artery. On the other hand, due to Bernoulli effect, the pressure in the stenosis would be reduced more, allowing the vessel to constrict even further.

Vasodilation Experimental studies dealing with the effect of vasodilation on flow in coronary arteries with eccentric lesions have demonstrated great changes in the resistance following vasodilation distal to stenosis. The same studies reported that, paradoxically, vasodilation caused flow either to remain constant or to decrease.

Schwartz et al. (1979) studied the effects of vasodilation on partially occluded canine coronary arteries. Vasodilation was induced by transient artery occlusion, distal to stenosis. Vasodilation caused flow to decrease and stenotic resistance to increase. Schwartz et al., proposed that the increase to stenotic resistance was a result of a passive decrease in stenotic area which follows reductions in the intraluminal pressure. Gould (1978) observed similar behavior for coronary arterial stenosis, after vasodilation. Gould, attributed the increase in stenotic resistance to the dilation of the adjacent arterial segment; the relative percent narrowing becomes more severe and the divergence angle increases. The same year, however, Lipscomb and Hooten (1978) published their results of

studies on stenosis geometry, suggesting that the exit angle does not affect the stenosis severity significantly.

Effect of intraluminal pressure Logan (1975)

performed a series of in-vitro experiments on post-mortem human coronary arteries. He observed that in arteries with eccentric lesions, an increase in the perfusion pressure, caused a decrease in resistance to flow and vice-versa. On the other hand, for rigid stenoses, perfusion pressure seemed to have no effect on the stenotic resistance. Using different experimental procedures, Schwartz et al. (1980) confirmed the dependence of stenotic performance on perfusion pressure. It was shown that increased aortic pressure could cause a decrease in the hemodynamic severity of the stenosis. In their conclusions, both studies suggested that, for compliant stenoses, the intraluminal pressure through the passive distension of the arterial wall, controls the severity of the stenosis.

Models of compliant arterial stenosis Recently,

Santamore and Bove (1985) developed a theoretical model for the compliant arterial stenosis. Although the model applies only to steady flow, it includes important variables such as vasomotor tone, intraluminal pressure, and compliance.

To incorporate the effect of the intraluminal pressure in the model, Santamore and Bove used an approximate, non-

linear relation between intraluminal pressure and the circumference of the tube. To account for the partial rigidity of the tube, the circumference value was weighted proportionally to the elastic portion of the stenosis wall. A sensitivity factor was introduced to account for the various types of plaque shape. Vasoconstriction was taken to cause approximately 20% decrease in vessel circumference, at pressures under 100 mm Hg and to have no effect at pressures above 150 mm Hg.

Santamore and Bove recognized that the transluminal distending pressure would change across the stenosis, resulting in different luminal areas at different longitudinal positions. To correct for this effect, they divided the stenosis length into a number of segments where a single value for the transluminal pressure is applied. The resulting system of equations was solved on a computer using an iterative technique.

The model describes well the characteristics of flow through compliant stenosis. Solutions given by the theoretical model for various hypothetical situations agree, at least qualitatively, with experimental data. Vasoconstriction always reduced flow. Increased intraluminal pressure increased flow. The paradox of decreased flow following a decrease in distal resistance was also demonstrated.

Besides giving a reasonable, simple theoretical model for the compliant stenosis, the study emphasized the importance of the characteristics of the arterial lesion. However, this becomes its limiting point, because in general these characteristics are not known.

Dubill (1986) also studied the steady flow case by performing experiments on models of compliant stenoses. Model stenoses consisted of an asymmetric rigid plug inserted into thin-walled latex tubing. A portion of the stenosis wall was free to respond to changes in transmural pressure, when the model was placed in an airtight chamber, resembling the Starling resistor device. Steady flow tests were conducted for a wide range of Reynolds numbers and for three different values of percent stenosis (75%, 85%, and 89%).

The results agreed well with those from previous studies on collapsible tubes. When the tube was in the uncollapsed state, flow behaved essentially as in a rigid tube. When the transmural pressure exceeded a critical point, the tube collapsed and flow did not increase with further reductions on the distal pressure. A typical set of experimental flow-pressure curves for the 85% stenoses are shown in Fig. 8. Dubill also showed that, when the tube is collapsed, the maximum flow rate,  $Q$ , was a linear function

of  $P_1 - P_e$  and the effective severity of the collapsed segment increased markedly at high values of transmural pressures.

In conclusion, this study demonstrated that indeed compliant stenoses behave dynamically. Thus, it seems likely that under clinical conditions of reduced intraluminal pressure, resulting from vasodilation, compliant stenoses can collapse, thereby limiting the perfusion to the peripheral beds and leading to ischemia.

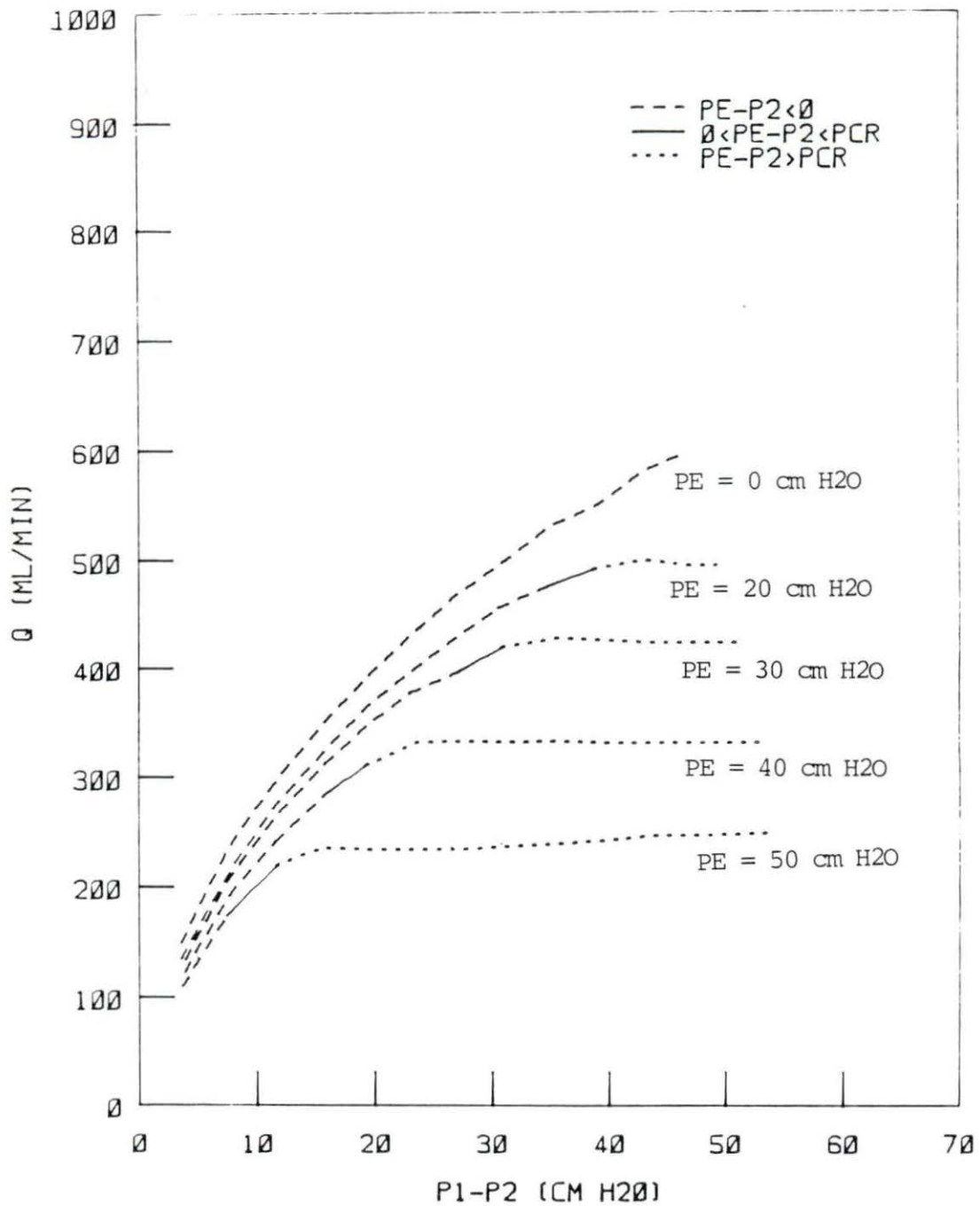


FIGURE 8. Pressure-flow curves for 85% stenosis, at different external pressures. The dotted line denotes stenosis in collapsed state. From Dubill, 1986

## MATHEMATICAL MODEL

One of the major objectives of this study, was to develop a simple theoretical model for the pulsating flow through a compliant stenosis. The approach followed was to modify the already existing models for rigid stenoses to incorporate the effects of the stenosis compliance. This section discusses the individual steps used in the development of the mathematical model.

## Rigid Stenosis Models

As mentioned in the Literature Review, Young and Tsai (1973b) developed the empirical relationship for the pulsatile flow through rigid stenoses in the form

$$\Delta p = \frac{4K_v \mu}{\pi d^3} Q + \frac{8K_t \rho}{\pi^2 d^4} \left[ \frac{A_0}{A_1} - 1 \right]^2 Q^2 + \frac{4K_u \rho L}{\pi d^2} \frac{dQ}{dt} \quad (5)$$

where:

$\Delta p$  = pressure drop across the stenosis

$Q$  = volume rate of flow

$d$  = diameter of the unobstructed tube

$\mu$  = viscosity of the fluid

$\rho$  = density of the fluid

$A_0$  = cross-sectional area of unobstructed tube

$A_1$  = minimum free cross-sectional area of the stenosis

For severe stenoses the third term of Eq. 5 is considered insignificant, and therefore is usually omitted. The coefficient  $K_t$ , as proposed by Young et al. (1976) is only slightly dependent on geometry and has been approximated with the constant value of 1.52. It can be shown theoretically that  $K_t$  is equal to 1.5 for ideally blunt stenoses. Therefore, the value of 1.5 can be substituted for  $K_t$ , without introducing significant error.

The coefficient  $K_v$  depends greatly on the geometry of the stenosis. Seeley and Young (1976) developed the relationship

$$K_v = 32 \left( \frac{L_a}{d} \right) \left( \frac{A_o}{A_1} \right)^2 \quad (6)$$

for  $K_v$  where,  $L_a$ , is a modified length of the stenosis to account for the entrance and exit effects. However, since Eq. 6 was developed for stenoses of circular cross-section, it is envisioned that for non-circular cross-sections, as in the stenoses used in the present study, a correction factor,  $\beta$ , should be introduced. Thus, Eq. 6 is rewritten as

$$K_v = 32\beta \left( \frac{L}{d} \right) \left( \frac{A_o}{A_1} \right)^2 \quad (7)$$

where  $\beta$  is assumed also to account for the entrance-exit effects, so that the actual length of stenosis,  $L$ , is used in Eq. 7.

With these assumptions Eq. 4, for the pressure drop, can be expressed as

$$\Delta p = 128\beta \left(\frac{L}{d}\right) \left(\frac{A_0}{A_1}\right)^2 \frac{\mu}{\pi d^3} Q + \frac{12\rho}{\pi^2 d^4} \left[\frac{A_0}{A_1} - 1\right]^2 Q^2 \quad (8)$$

and this relationship is expected to be valid for rigid stenoses. The last term in Eq. 5 has been neglected.

#### Effects of Compliance - Pressure-Area Relation

Vessel wall compliance allows the stenosis to alter its geometry, as a response to changes in pressure. A simple way to model the effects of compliance is through a relation between the pressure and the free area of the stenosis. If the relationship is assumed to be linear it follows that

$$A_i(x) = A^* + C(p_i(x) - p^*) \quad (9)$$

where:

$p_i(x)$  = the pressure at a particular cross section of the stenotic region ( $x$  is a longitudinal coordinate)

$A_i(x)$  = free area at the particular cross-section within the stenosis

$A^*$  = free area of the stenosis corresponding

to a perfectly circular arc for the compliant wall segment (which is the configuration when  $p_i(x)=p^*$ )  
 $p^*$  = reference pressure at which  $A_i$  is equal to  $A^*$   
 $C$  = incremental compliance

Equation 9, although simple in form, suggests that the free cross-sectional area will be changing along the stenosis (following changes in the local pressure) due to the continuous pressure drop along the stenosis. Thus, rather than having a single value for the free cross-sectional area throughout the stenosis, the cross-sectional area would actually depend on position within the stenosis. However, to be able to combine Eq. 9 with Eq. 8, which holds for the entire stenosis length, Eq. 9 is modified to

$$A_i = A^* + C(p_i - p^*) \quad (10)$$

where  $A_i$  now represents the average free cross-sectional area, and  $p_i$  is the average pressure within the stenosis.

Equation 10 can be divided by  $A_0$ , the cross-sectional area of the unobstructed tube, to yield

$$\frac{A_i}{A_0} = \frac{A^*}{A_0} + \frac{C}{A_0}(p_i - p^*) \quad (11)$$

It is to be noted that

$$(1 - A^*/A_0) \times 100 = \text{percent area stenosis at reference pressure, } p^*, \text{ and}$$

$(1-A_i/A_o) \times 100 =$  percent area stenosis at pressure,  $p_i$ .

Because the pressure inside the stenosis,  $p_i$ , is an unknown variable, use of the Bernoulli equation was made to develop an approximate explicit relationship between  $p_i$  and the pressure,  $p_1$ , which is proximal to the stenosis.

According to the Bernoulli equation

$$p_1 + \frac{\rho}{2} V_1^2 = p_i + \frac{\rho}{2} V_i^2 \quad (12)$$

Eq. 12 can be combined with the continuity equation

$$Q = V_i A_i = V_1 A_o \quad (13)$$

to yield

$$p_i = p_1 - \frac{\rho}{2} \left( \frac{1}{A_i^2} - \frac{1}{A_o^2} \right) Q^2 \quad (14)$$

Although the Bernoulli equation, as expressed in Eq. 14, is valid only for steady, non-viscous flow, it is thought to provide a reasonable approximation because it is applied in the converging portion of the stenosis. In such a case the pressure drop from  $p_1$  to  $p_i$  due to the Bernoulli effect is much larger than that due to viscous effects. Equation 14 can be simplified further by replacing the variable  $A_i$  by its time mean value  $A_{i_m}$ , recognizing that the

substitution will not affect the shape of the  $p_i$  waveform significantly. The final expression for the pressure inside the stenosis becomes

$$p_i = p_1 - \frac{\rho}{2} \left( \frac{1}{A_{im}} - \frac{1}{A_o} \right)^2 Q^2 \quad (15)$$

### The Mathematical Model

Equations 8, 11, and 15 can be combined to yield the proposed mathematical model for the compliant stenosis

$$\begin{aligned} \Delta p = & 128\beta \left( \frac{L}{d} \right) \left( \frac{\mu}{\pi d^3} \right) \left[ \frac{A^*}{A_o} + \frac{C}{A_o} (p_i - p^*) \right]^{-2} Q \\ & + \frac{12\rho}{\pi^2 d^4} \left[ \left( \frac{A^*}{A_o} + \frac{C}{A_o} (p_i - p^*) \right)^{-1} - 1 \right]^2 Q^2 \end{aligned} \quad (16)$$

with  $p_i$  given by Eq. 15.

Equation 16 is the empirical relationship proposed to describe the fluid mechanics of the compliant stenosis. In order to apply the equation, the three parameters that enter the equation,  $\beta$ ,  $p^*$ , and  $C/A_o$  must be defined. The procedures for defining the parameters as well as the results of the application of the mathematical model to the

experimental data, are given in the chapters titled 'Materials and Procedures' and 'Results and Discussions'.

## MATERIALS AND PROCEDURES

To investigate the fluid mechanics of pulsatile flow through a compliant stenosis, a simple hydraulic model driven by a piston-type pulsating mechanism was used. For better comparison with steady flow test results, the experimental set-up and the materials used in the present study were the same as those used by Dubill (1986). A discussion of the materials used, the experimental set-up, and the experimental procedures is given in the following sections.

### Materials

A single type of stenosed segment was used, and a photograph of this segment is shown in Fig. 9. A schematic representation of the stenosed segment, showing the position of the stenosis in the compliant segment, the dimensions of the segment, and the way that the compliant segment is attached to the rigid tube of the flow system, is shown in Fig. 10.

Because of their particular importance to the mechanical behavior of the system, the stenosis characteristics, the collapsible tube properties, and the properties of the fluid used are described separately below.

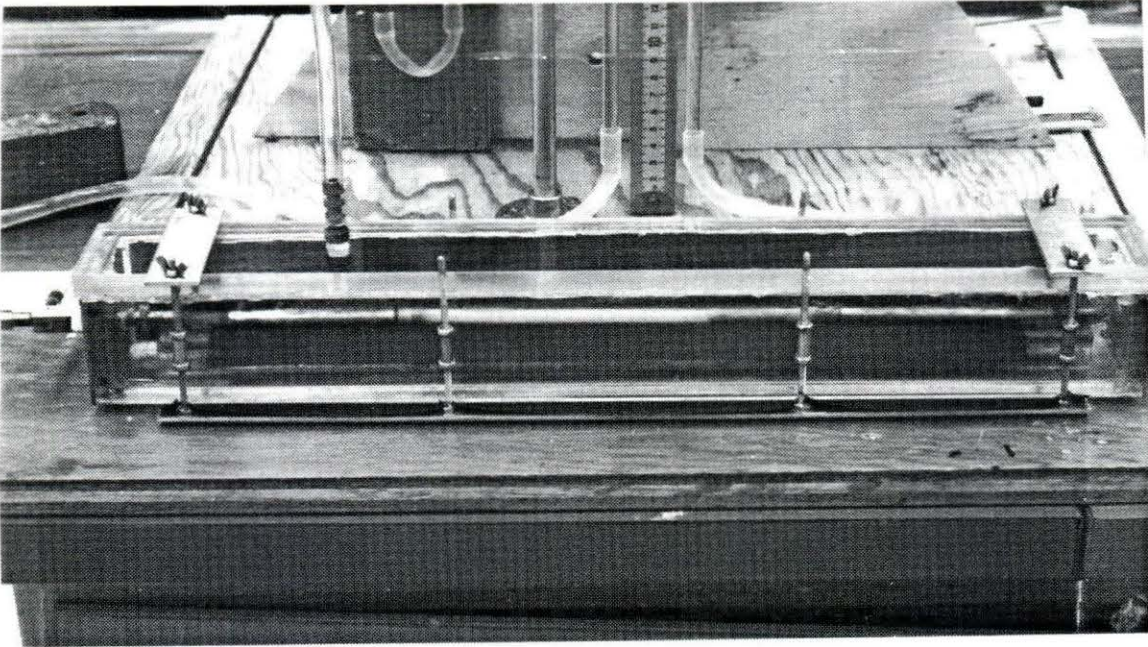


FIGURE 9. Photograph of the stenosed segment

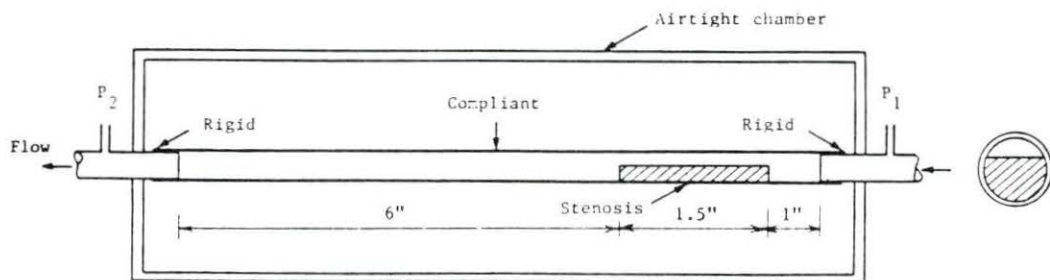


FIGURE 10. Schematic representation of the stenosed segment

### Stenosis characteristics

Three stenoses of different severity (74%, 84%, and 88% area reduction) were used in attempt to have both critical (84 and 88%) and subcritical (74%) stenoses. Figure 11 shows a schematic representation of the stenoses. The length,  $L$ , of all stenoses was 1.5 inches. All stenoses were manufactured from a brass rod, having a diameter,  $d$ , of 0.23 inches, equal to the nominal internal diameter of the elastic tube in which the stenoses were placed. The height,  $h$ , was different for each stenosis, and selected to give the desired percent area reduction.

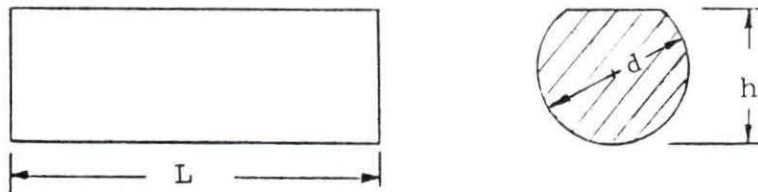


FIGURE 11. Stenosis characteristics

### Collapsible tube properties

The collapsible tubing used was x-ray opaque Penrose drain tubing. As described by Dubill (1986), the tube has an internal diameter,  $d$ , of 0.23 inches and a thickness,  $t$ ,

of approximately 0.012 inches, thus giving a  $t/d$  of about 0.052, which is a value that is typical of some systemic arteries. The modulus of elasticity,  $E$ , and the Poisson ratio,  $\nu$ , had values of 178 psi and 0.5, respectively (Holmberg and Wilson, 1970). The value of the Poisson's ratio is typical of most of the systemic arteries, and the value of  $E$  is close to that of human pulmonary artery.

The mechanical properties of the tubing changed after continuous exposure to air and light, so fresh tubing was always used in the tests, with the maximum period of exposure to air and light being two days.

#### Fluid properties

For all tests, water at a constant temperature of  $25^{\circ}\text{C}$  was used. At this temperature, water viscosity is  $8.9 \times 10^{-4}$   $\text{Ns/m}^2$ , and water density is  $997 \text{ kg/m}^3$ , as specified by Weast (1976).

#### Experimental Set-Up

The experimental set-up consisted of two major parts: the flow system and the data acquisition system.

#### Flow system

A general photographic view of the flow system is given in Fig. 12. The function as well as the various components

of the flow system are illustrated schematically in Fig. 13. The test section that appears in Fig. 13 was drawn in detail in Fig. 10 and contains the stenosed segment with the flexible tube.

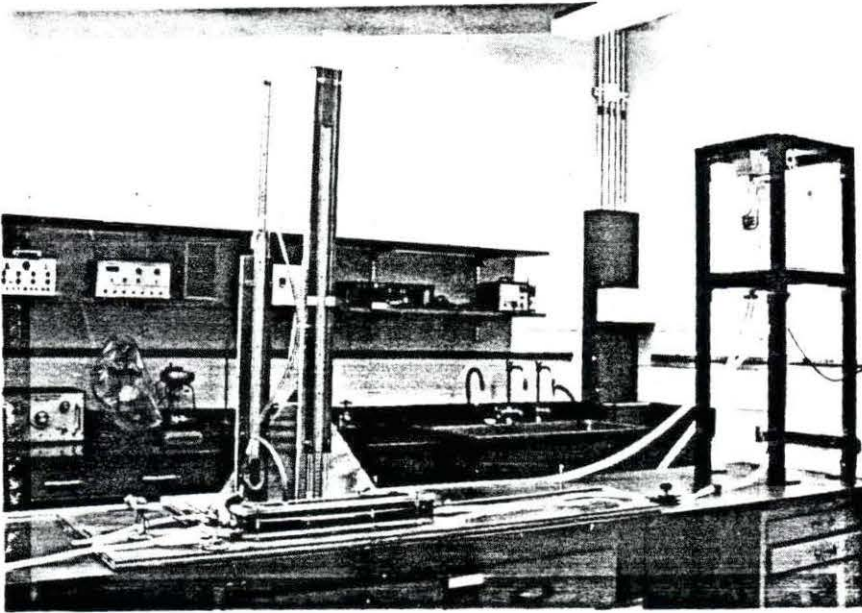


FIGURE 12. Photograph of the flow system

The two resistances  $R_1$  and  $R_2$  were used to control the flow at the desired level (control of mean Reynolds number) as well as to control the mean values of pressure proximal and distal to the stenosis. The flow straightener was a rigid tube, sufficiently long ( $l > 100d$ ) to let the flow fully develop before entering the test section. The pulsatile pump consisted of a piston-cylinder combination, driven by

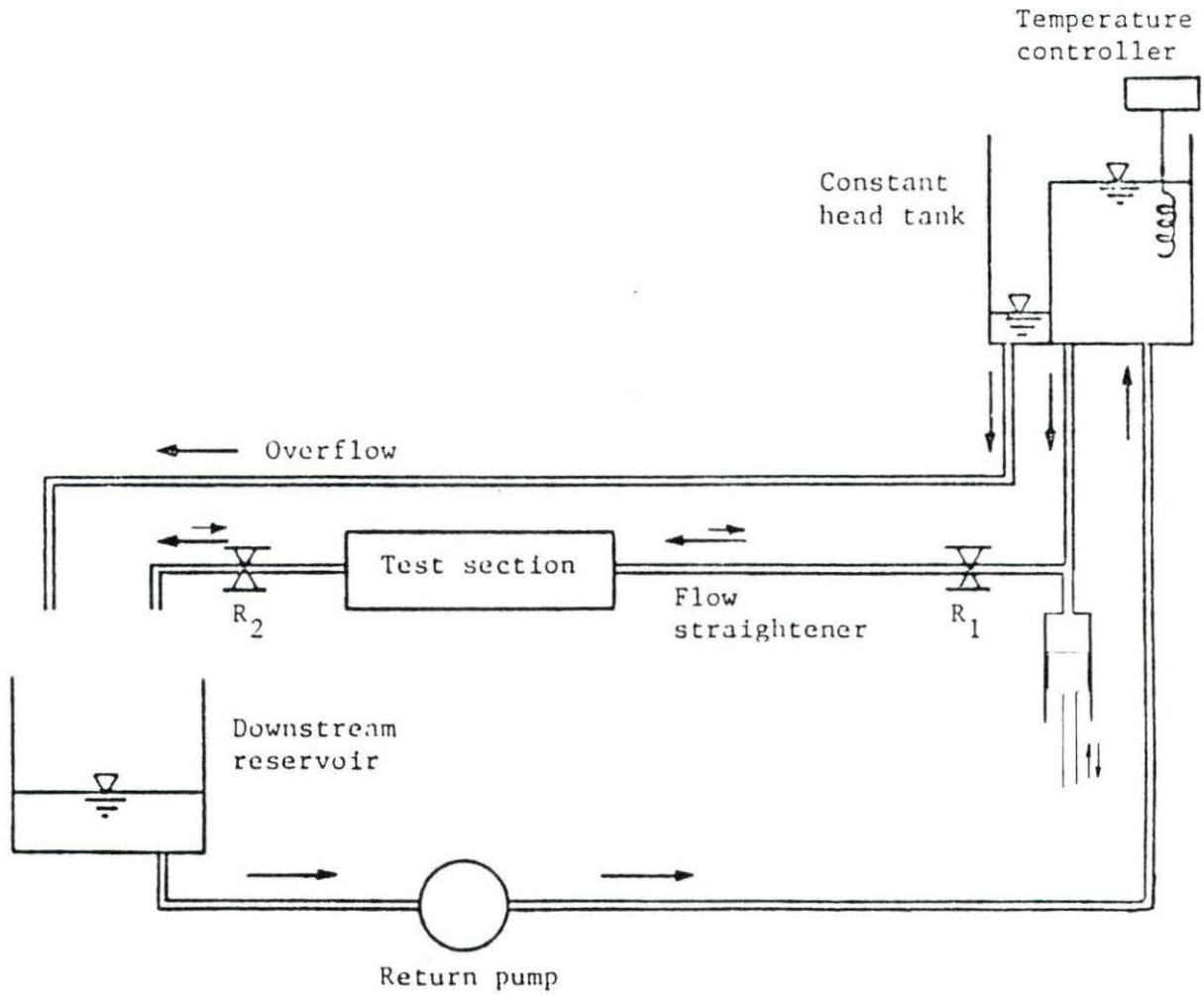


FIGURE 13. Schematic diagram of the flow system

an electric motor. The electric motor was controlled by a controller which enables precise frequency selection in the range of 0 to 300 rpm.

#### Data acquisition system

The data acquisition system was designed to obtain the proximal pressure,  $p_1$ , distal pressure,  $p_2$ , and flow,  $Q$ , digitize those values, and store them for later analysis. The data acquisition system consisted of the pressure and flow transducers and their associated electronics, an analog-to-digital converter, and a micro-computer.

Sensing devices Proximal and distal pressures were measured using Statham P23Dc strain gage pressure transducers. Flow was measured with an electromagnetic Biotronex BL-610 Pulsed Logic flowmeter.

Amplifier The signals were amplified by a Grass Polygraph Recorder.

Digitizer and micro-computer To convert the electric signals from the amplifier to digital signals for further analysis, a high-speed analog-to-digital converter (KEITHLEY data acquisition system) along with the supporting software (SOFT500), were employed. The micro-computer used for coordinating the whole process and storing the data was an IBM PC-AT computer.

## Procedures

The whole experimental procedure was divided into two phases. In phase one, the pulsatile flow tests were run, and the data collected were stored in the computer. In phase two, the data processing took place, which involved mathematical and statistical analysis of the stored data.

### Pulsatile flow tests

Pulsatile flow tests were run for three different  $a$  values, for each of the three stenoses (74%, 84%, and 88%). For each stenosis, a step by step procedure was followed. The individual steps involved: preparing the stenosis, calibrating the equipment, and running the pulsatile flow tests.

Stenosis preparation      The stenosis was created by inserting the fabricated brass rod (see Fig. 11) in the flexible tubing, at the desired position. Rather than being glued to the tubing, the rod was stabilized in the tubing by means of an external clamp.

Because different stenosis preparations would lead to different severities, for each stenosis preparation a standardizing procedure was followed. The procedure involved steady flow through the stenosis, with the flow and corresponding pressure drop across the stenosis measured.

The stenosis was readjusted until for a given flow, the pressure drop was approximately (within 2%) the same as reported by Dubill (1986), for the same flow rate and the same stenosis severity. Once a suitable stenosis was obtained, the next step was to calibrate the equipment.

Equipment calibration      The equipment was calibrated by running steady flow tests, and assuming linearity for the signals coming from the pressure transducers and electromagnetic flowmeter. The values for the proximal,  $p_1$ , and distal,  $p_2$ , pressures were obtained from a piezometer tube. The values for the flow rate were obtained by measuring the filling time of a known volume, in a graduated cylinder. Different sets of pressures,  $p_1$  and  $p_2$ , and flow rates,  $Q$ , along with their corresponding digitized values,  $p_{1d}$ ,  $p_{2d}$ , and  $Q_d$ , were obtained by adjusting the resistances  $R_1$  and  $R_2$ . Finally, linear regression was applied to each of the pairs,  $(p_1, p_{1d})$ ,  $(p_2, p_{2d})$ , and  $(Q, Q_d)$  to give the relationship between the variables. The regression procedure was considered successful when the correlation coefficient,  $R^2$ , was greater than 0.99; if not, the calibration procedure was repeated.

Pulsatile flow tests      Four different sets of data for each stenosis were taken. For the first three data sets, the tube was in an uncollapsed state. Each of the

three data sets corresponded to a different  $\alpha$  value, all of which were in the range  $4 < \alpha < 7$ . The mean Reynolds numbers for all alpha values and stenoses ranged between 1000 and 1500. The  $\alpha$  value adjustment was done by changing the frequency of the pulsating mechanism. The last data set was obtained when the tube was partially or completely collapsed. Collapse was achieved by reducing the distal resistance. The data set was taken at high  $\alpha$  values ( $6.2 < \alpha < 7.0$ ), and was taken for a qualitative, rather than a quantitative or mathematical, analysis of the phenomenon.

The sampling rate was chosen to be either 100 or 200 Hz (sampling interval 10 or 5 msec). The sampling rate was high enough to provide 200 to 350 points per cycle; a sufficient resolution for the filtering and statistical procedures that followed.

#### Data Processing

The raw data stored in the computer were processed following a step by step procedure which included signal averaging and filtering, pressure drop calculation, and finally, statistical analysis.

### Signal averaging and filtering

Signal averaging was performed for two reasons: First, it reduced the effect of system noise on the sampled data, and second, it provided a single, complete waveform which was necessary for the numerical method used in the pressure drop calculation. Also, with the signal averaging technique, the average period of the oscillation was identified and was used to calculate important parameters of the problem, such as the alpha parameter,  $\alpha$ , and the mean Reynolds number,  $\overline{Re}$ .

Filtering of the waveforms was done with the use of low-pass digital filters. The cut-off frequency was approximately 30 Hz, which was sufficiently low to eliminate the 60 Hz noise, and high enough not to alter the amplitude of the low frequency components of the true signal.

### Pressure drop calculation

From the known proximal,  $p_1(t)$ , and distal,  $p_2(t)$ , pressure waveforms, the instantaneous pressure drop waveform,  $\Delta p(t) = p_1(t) - p_2(t)$ , could be obtained. However, this pressure drop is a sum of the pressure drop due to stenosis and the pressure drop due to flow in the remaining section of the tube between the two measuring points. Since the pressure drop due to stenosis,  $\Delta p_S$ , is of prime concern, the pressure drop due to flow in the tube,

$\Delta p_f$ , (without stenosis) was calculated and subtracted from the total pressure drop, in accordance with the equation

$$\Delta p_s(t) = \Delta p(t) - \Delta p_f(t) \quad (14)$$

To obtain  $\Delta p_f$  the problem of pulsatile flow in a straight, rigid tube had to be solved. The problem was solved with a numerical technique based on finite difference analysis. Details on the formulation of this problem and the numerical technique are given in the Appendix.

#### Parameter estimation - Statistical analysis

Once the waveforms  $\Delta p_s(t)$  and  $Q(t)$  were known, a statistical analysis was performed, to assess the validity of the theoretical model, and to estimate the parameters of the model.

Estimation of  $p^*$  The parameter,  $p^*$ , could not be accurately estimated due to its strong correlation with the correction factor,  $\beta$ . Attempts to estimate  $p^*$  and  $\beta$  simultaneously led to oscillating estimates and non-convergence of the non-linear regression scheme, which suggested that to apply statistical analysis to obtain the other parameters, one of the two parameters ( $p^*, \beta$ ) would need to be specified.

Although an attempt was made to get estimates of  $p^*$  by direct measurements of the external diameter of the stenosed

segment at different internal pressures (and correlating the  $p^*$  with the pressure for perfect circular configuration), the tests failed to give consistent and reliable values for  $p^*$ . The tests failed primarily because the small changes in vessel diameter could not be accurately measured with the equipment available.

Estimation of  $\beta$  and  $C/A_0$  With an assumed value of  $p^*$  (for demonstration purposes it was assumed that  $p^*$  equaled 35 cm H<sub>2</sub>O for the 82% and 88% stenosis, and 25 cm H<sub>2</sub>O for the 74% stenosis), statistical analysis for the evaluation of  $\beta$  and  $C/A_0$  could be applied if the time averaged cross-sectional area,  $A_{i_m}$ , is specified.  $A_{i_m}$  cannot be calculated directly from Eq. 11 because  $p_i(t)$  as given by Eq. 15 depends on the unknown value of the parameter  $A_{i_m}$ . To overcome this obstacle, the following iterative technique was used:

- Assume a reasonable initial value for  $A_{i_m}$  ( $A_{i_m} = A^*$ )
- Based on the assigned values for  $p^*$  and  $A_{i_m}$ , perform statistical analysis to get the best estimates for  $\beta$  and  $C/A_0$
- Substitute the value of  $C/A_0$  into Eq. 11 to get the  $A_i$  waveform and in turn the new value for  $A_{i_m}$
- Repeat steps 2 and 3 until the values for  $A_{i_m}$  converge

For the statistical analysis, the non-linear regression procedure of the SAS statistical package was used. The applicability of the mathematical model was judged by the goodness of the fit between the predicted and the measured waveforms, which was determined by means of residual squares and by plotting and comparing the waveforms.

#### Evaluation of the Experimental Set-Up

To ensure that the experimental set-up, the data acquisition system, and the supporting software operated properly, pulsatile flow tests were conducted and the acquired data were checked against the known theoretical solution for flow in straight, unobstructed rigid tube.

During these pulsating flow experiments, instantaneous flow,  $Q(t)$ , and pressure drop,  $p_1(t) - p_2(t)$ , over a specified length, were recorded and stored. Using a numerical technique that solves the problem of pulsatile flow in straight rigid tubes, the theoretical pressure drop over the same length of tube, and for the measured flow waveform, was calculated and compared with the measured pressure drop. The numerical method used for the calculation of the theoretical pressure drop is discussed in detail in Appendix A.

The experimental results are shown in Fig. 14, where the measured pressure drop (solid line) and the calculated pressure drop (broken line) are compared. The two curves compare well in terms of both amplitude and phase. The small phase lag between the two curves was thought to be mainly due to the phase delay of the electromagnetic flowmeter. However, the fit was considered to be satisfactory, suggesting that the experimental set-up was designed well, and was capable of undertaking similar experiments.

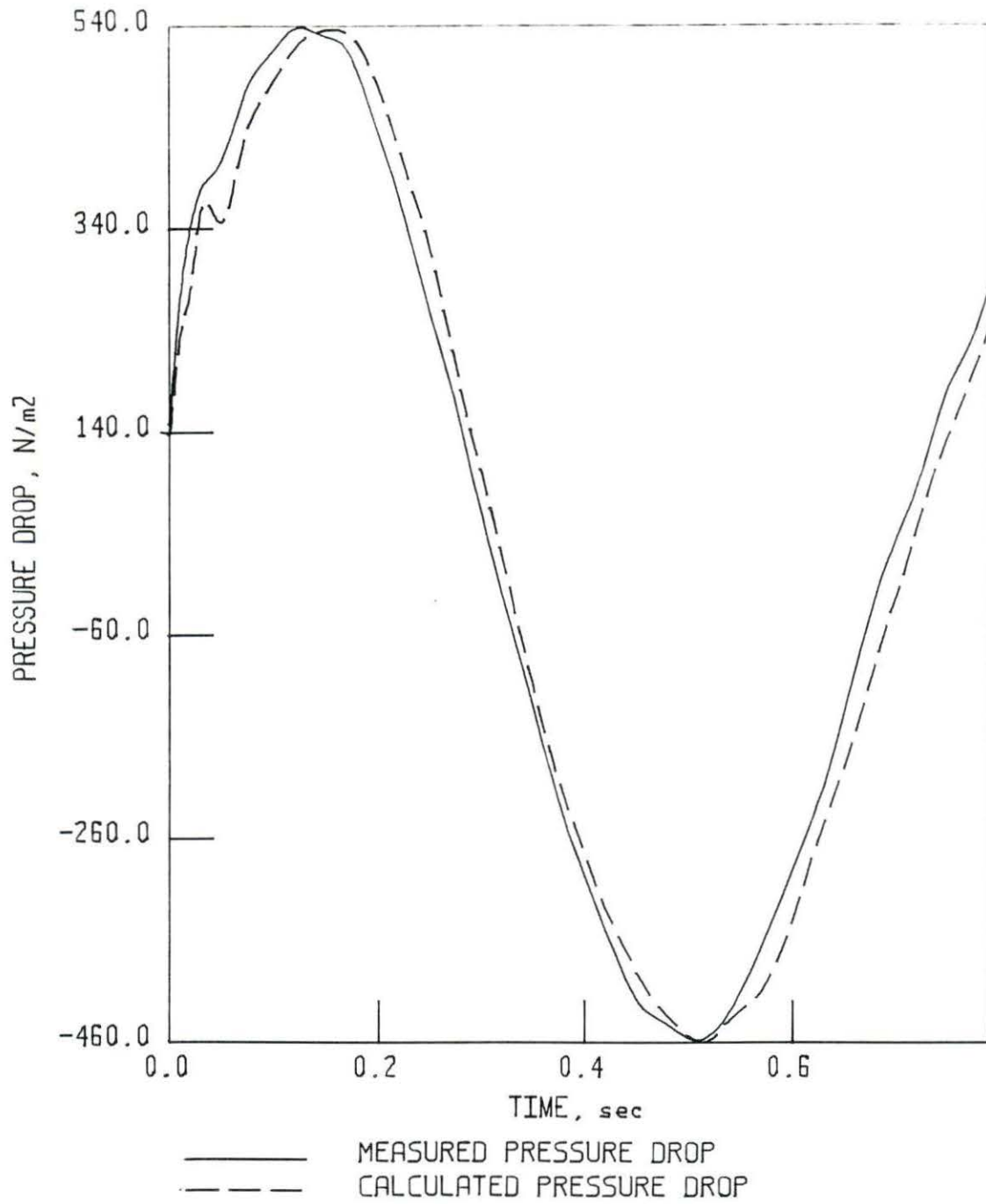


FIGURE 14. Theoretical vs measured pressure drop

## RESULTS AND DISCUSSION

The theoretical model developed was used in conjunction with the data collected from the pulsatile flow tests to check the validity of the model and to obtain estimates of the model parameters. A discussion of the results of the parameter estimation procedures, as well as a comparison between predicted pressure drop and experimental data is given in this chapter.

## Parameter Estimation

The three parameters that entered the model were the reference pressure,  $p^*$ , the correction factor,  $\beta$ , and the effective compliance,  $C/A_0$ . Although  $p^*$  was not estimated by running static tests, a certain region of  $p^*$  values was suggested ( $20 < p^* < 60$  in cm H<sub>2</sub>O) and for typical values of  $p^*$ ,  $\beta$  and  $C/A_0$  were estimated through a statistical analysis of the experimental data.

Estimation of  $\beta$  and  $C/A_0$ 

For the assumed  $p^*$  values,  $\beta$  and  $C/A_0$  were estimated by applying non-linear regression to  $Q(t)$  and  $\Delta P(t)$  waveforms, as they were expressed in the mathematical model (Eq. 16). The statistical procedure (SAS, NLIN Proc) was stable and always converged to the same values of  $\beta$  and  $C/A_0$ ,

regardless of the initial guess for the values of  $\beta$  and  $C/A_0$ . For the estimation procedure all sampled points (200-350 in number, depending on the period and sampling rate) were used. The estimated values for  $\beta$  and  $C/A_0$  for the three stenoses, along with the alpha values and the flow parameters  $\overline{Re}$  and PI (Pulsatility Index) corresponding to each set of data, are given on Table 1. The pulsatility index is defined as

$$PI = (Q_{\max} - Q_{\min})/Q_{\text{mean}}$$

The pulsatility index, PI, along with the mean Reynolds number and the alpha parameter,  $a$ , are the basic parameters needed to define pulsatile flow.

From the results of the parameter estimation the following conclusions can be drawn:

- For the severe stenoses (82% and 88%) and for the same stenosis preparation, the effective compliance,  $C/A_0$ , was essentially independent of the alpha value.
- The  $\beta$  values showed a slight dependence on the  $a$  parameter;  $\beta$  always decreased when  $a$  increased, that is when flow was more pulsatile.
- For the subcritical 74% stenosis, and for high alpha values ( $a > 5.5$ ), the effective compliance was

TABLE 1. Model and flow parameters for the non-collapsing pulsatile flow tests

Stenosis	$p^*$ cm H <sub>2</sub> O	$a$	$\beta$	$C/A_0^a$	$\overline{Re}$	PI
74%	25	4.8	2.52	0.57	1437	0.33
		5.9	1.08	0.01 <sup>b</sup>	1417	0.47
		6.7	0.93	0.00 <sup>b</sup>	1395	0.60
82%	35	4.7	3.09	1.45	1166	0.22
		5.9	2.91	1.43	1135	0.33
		6.4	2.89	1.50	1135	0.38
88%	35	4.5	3.43	0.60	1180	0.12
		5.9	3.26	0.57	1066	0.33
		6.4	3.24	0.61	1055	0.40

$$^a C/A_0 \times 10^{-5} \text{ in m}^2/\text{N}.$$

$$^b C/A_0 < 10^{-7}.$$

insignificant and the value of  $\beta$  was close to unity. However, for the low alpha value of 4.5,  $\beta$  was greater than one and the effective compliance had a significant value, comparable to those of the critical stenoses.

#### Theoretical vs Experimental Data

Figures 15-23 show the measured and the theoretical pressure drop across the stenosis, as predicted by Equation 16, using the estimated values for  $\beta$  and  $C/A_0$ . The

corresponding flow waveforms (only one for each stenosis) which were used as input to the theoretical model are shown in Figs. 24-26.

For all stenoses (74%, 82%, and 88%), and alpha values, the agreement between the measured and the theoretical pressure drop waveform was satisfactory. There was a small phase difference between the two waveforms which is partly attributed to the fact that inertial forces, which are always present, are neglected in the theoretical model. A significant part of the phase shift was also due to the electromagnetic flowmeter time delay; the measured flow waveform is shifted in time thus causing the calculated pressure drop waveform to be shifted (delayed). However, the phase lag was always less than  $10^{\circ}$ , and it was almost negligible for the 88% stenosis where the inertial forces were insignificant.

#### Significance of the Compliance

Compliance is responsible for changes in the cross-sectional area of the stenosis. Figures 27-29 show the way the ratio of the stenosis cross-sectional area to the area of the unobstructed tube,  $A_i/A_o$  changed over a cycle.

The fluctuation of  $A_i/A_o$  ranged from 3% over the mean value for the 74% stenosis to 4% and 7% for the 88% and 82%

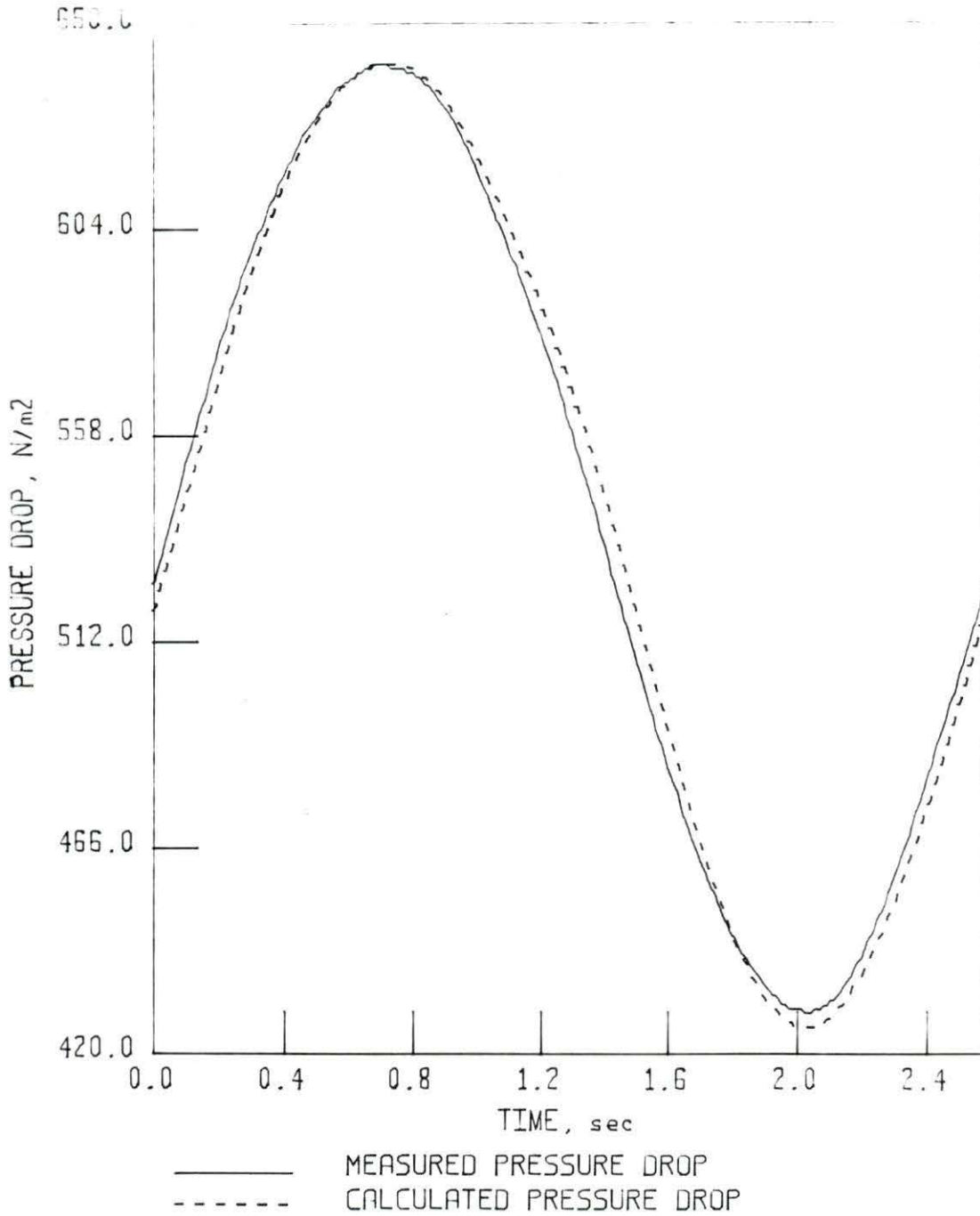


FIGURE 15. Pressure drop waveforms for the 74% stenosis ( $\alpha=4.7$ )

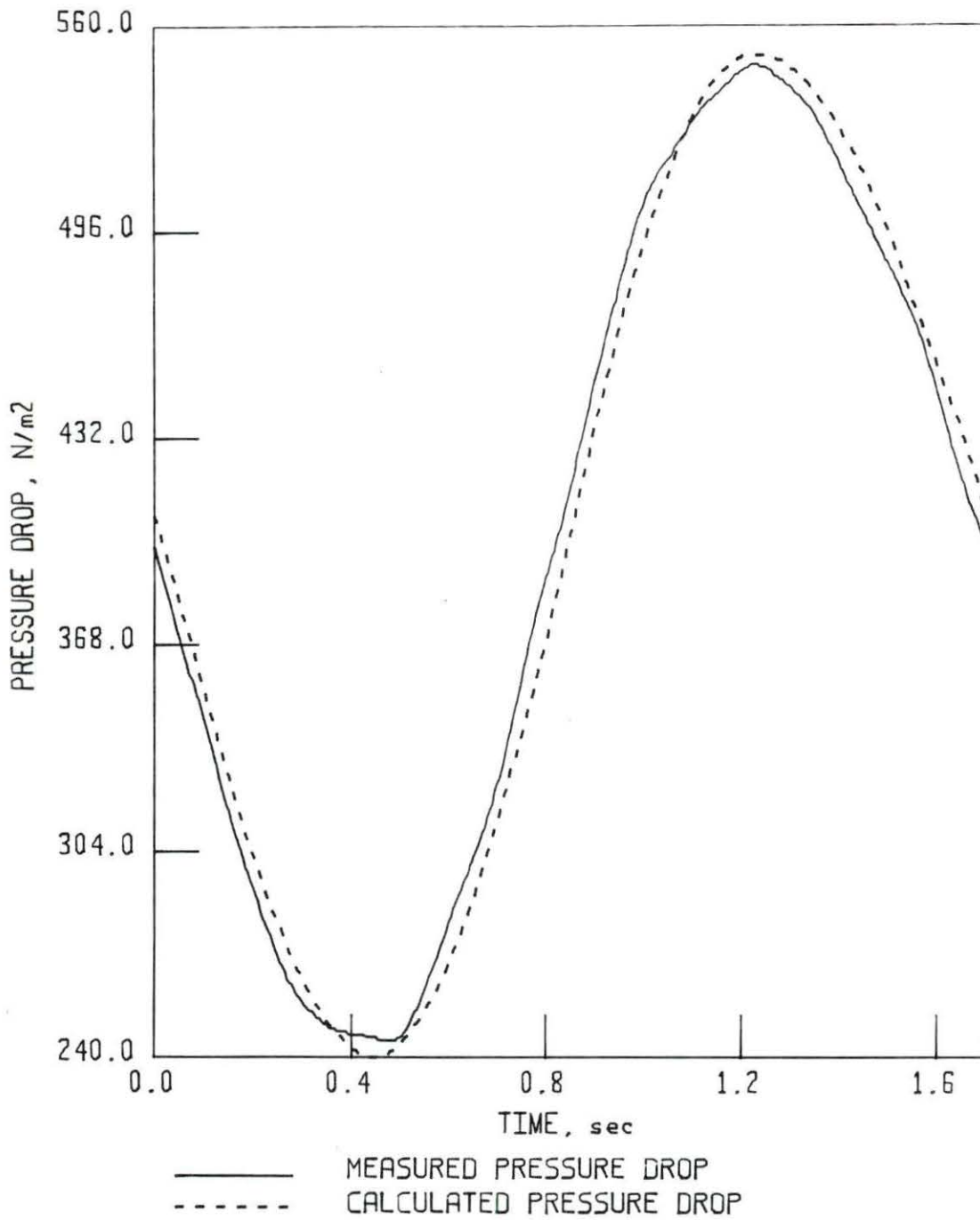


FIGURE 16. Pressure drop waveforms for the 74% stenosis ( $a=5.9$ )

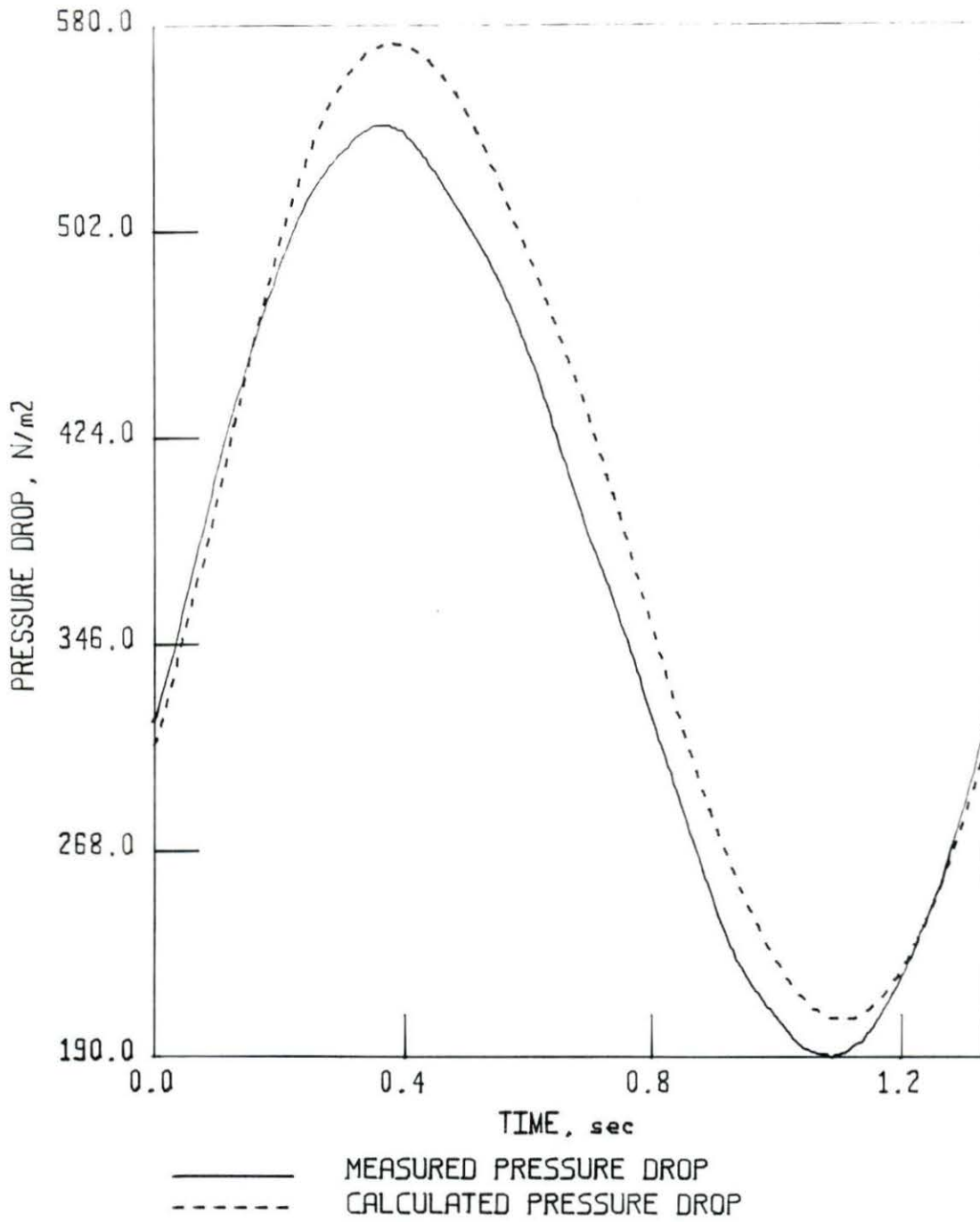


FIGURE 17. Pressure drop waveforms for the 74% stenosis ( $a=6.4$ )

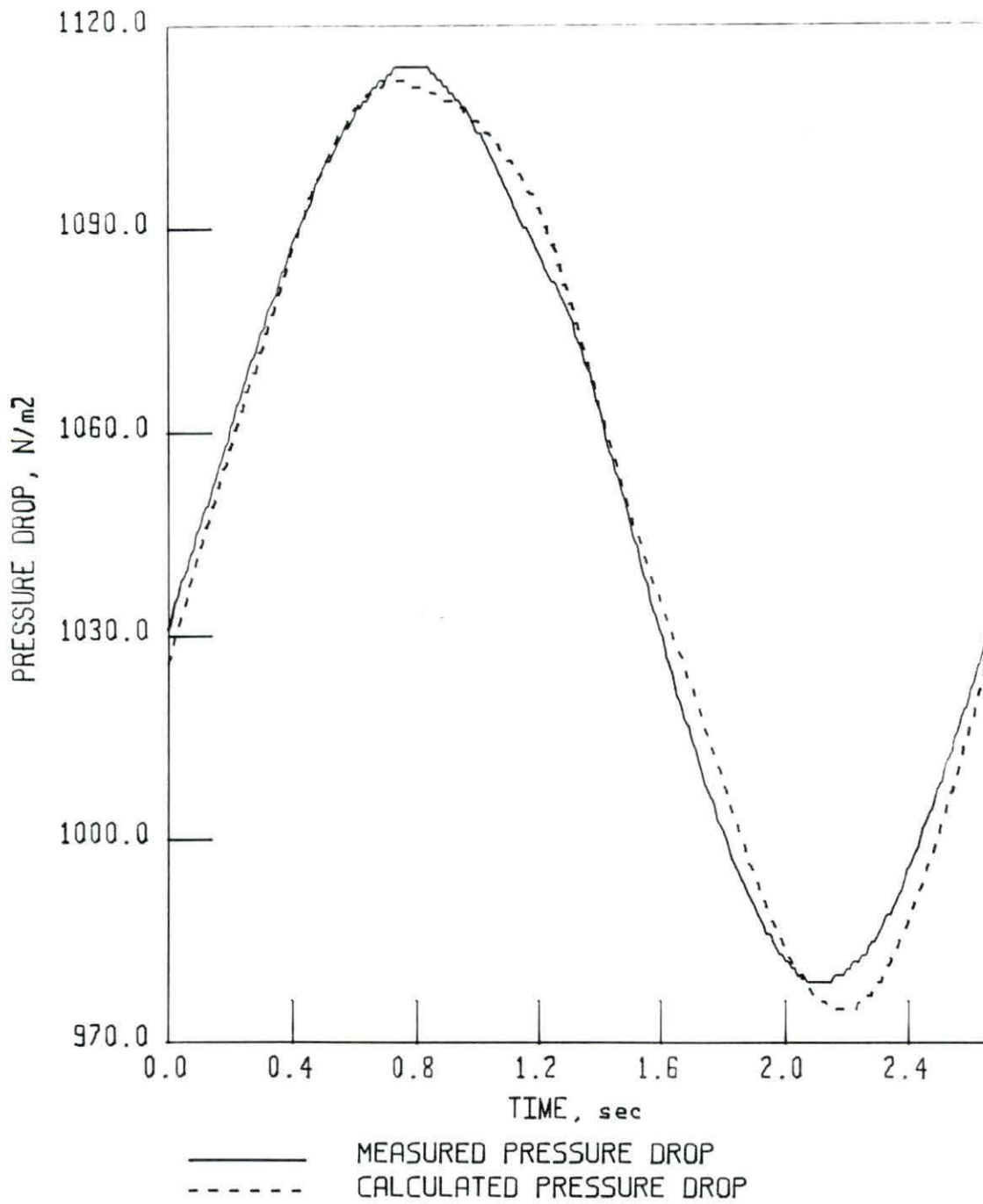


FIGURE 18. Pressure drop waveforms for the 82% stenosis ( $a=4.7$ )

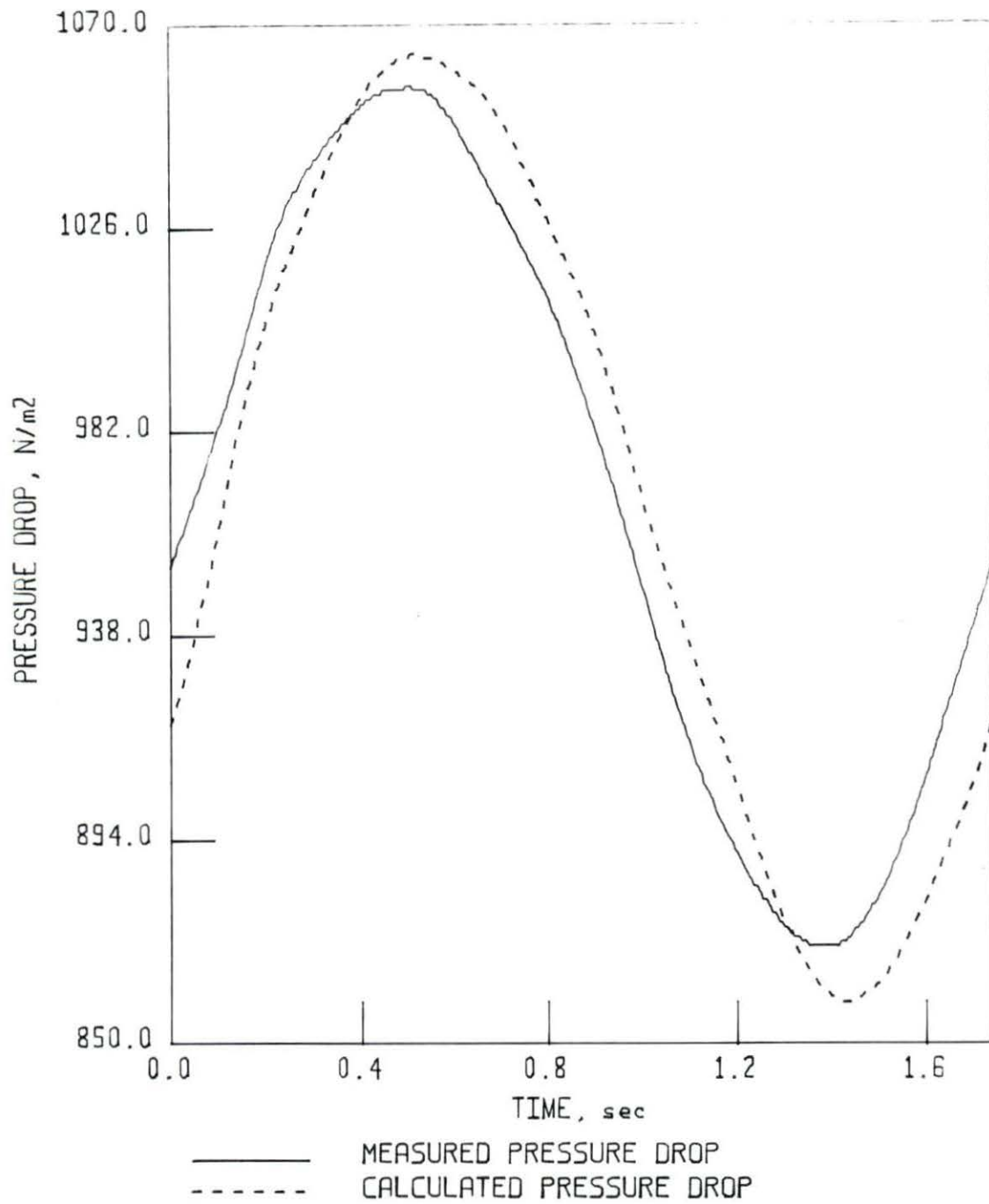


FIGURE 19. Pressure drop waveforms for the 82% stenosis ( $a=5.9$ )

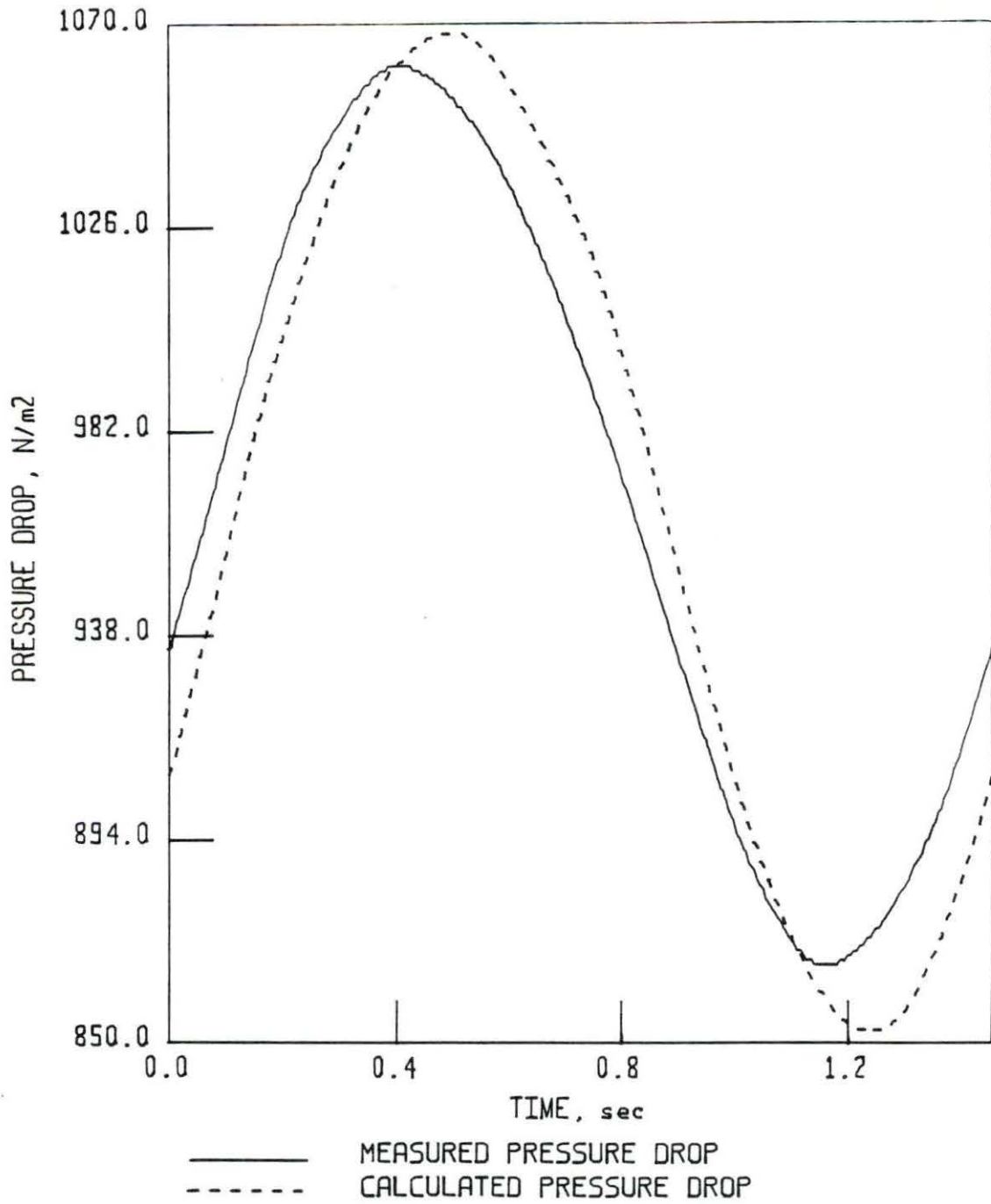


FIGURE 20. Pressure drop waveforms for the 82% stenosis ( $a=6.4$ )

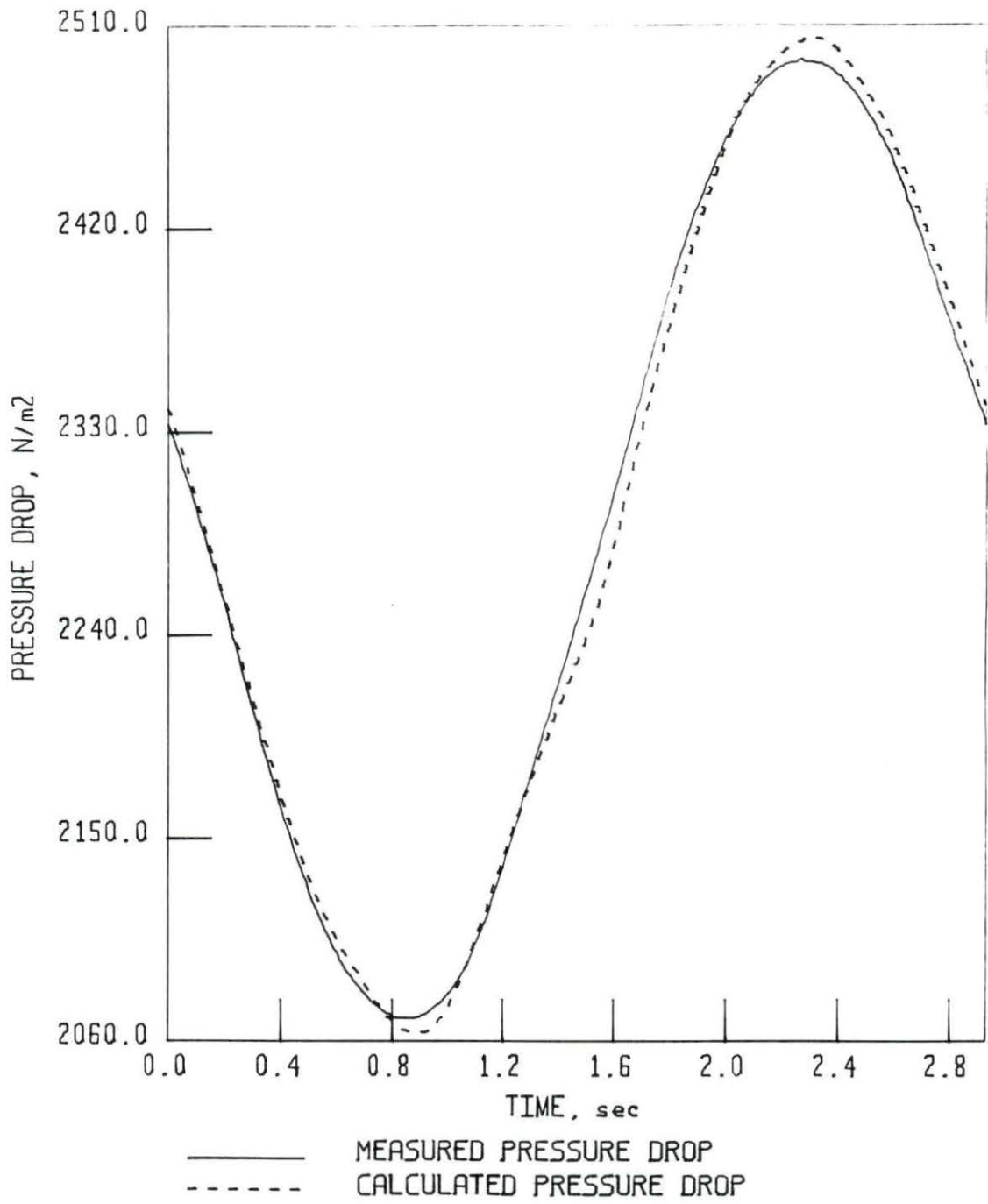


FIGURE 21. Pressure drop waveforms for the 88% stenosis ( $a=4.5$ )

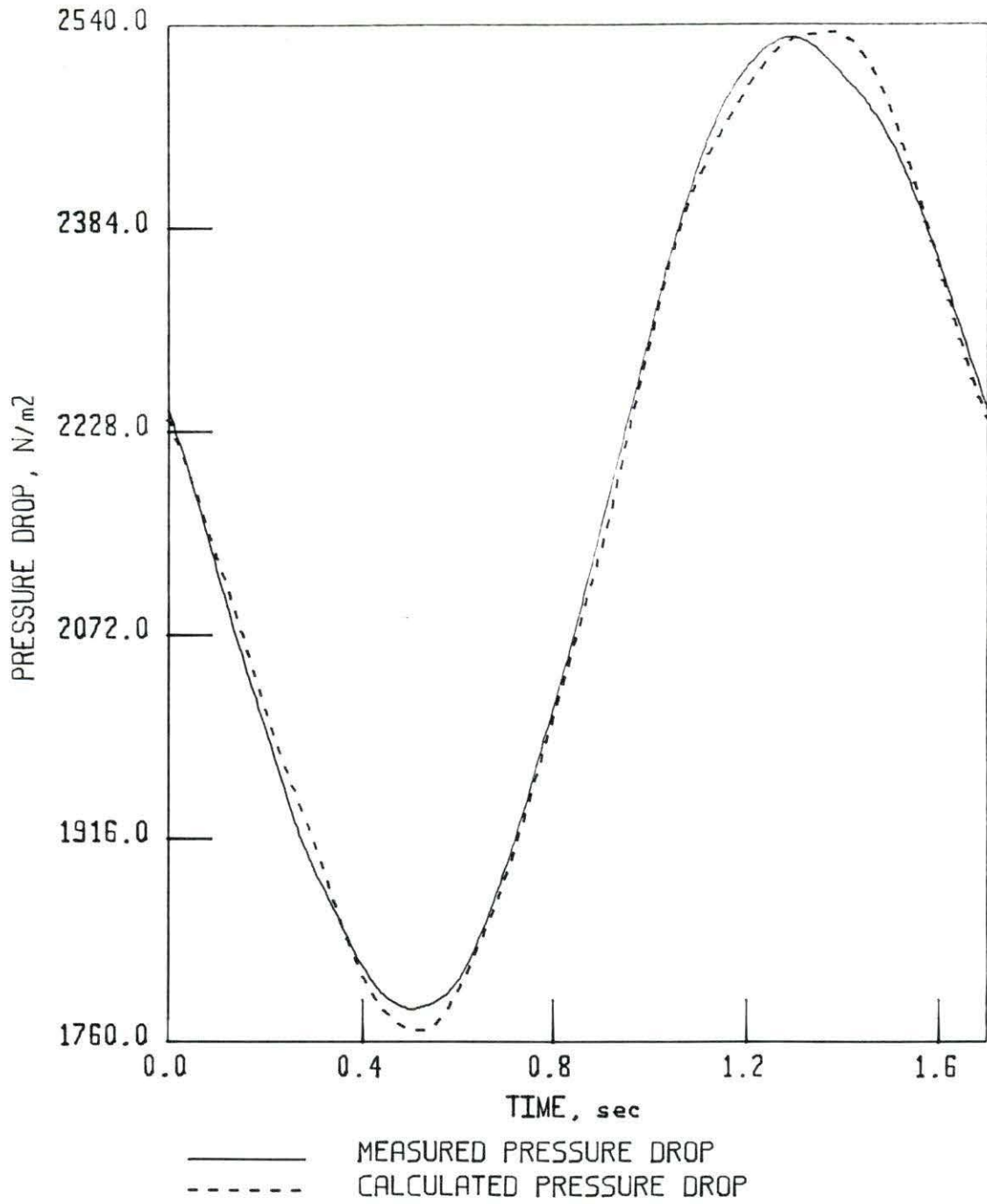


FIGURE 22. Pressure drop waveforms for the 88% stenosis ( $a=5.9$ )

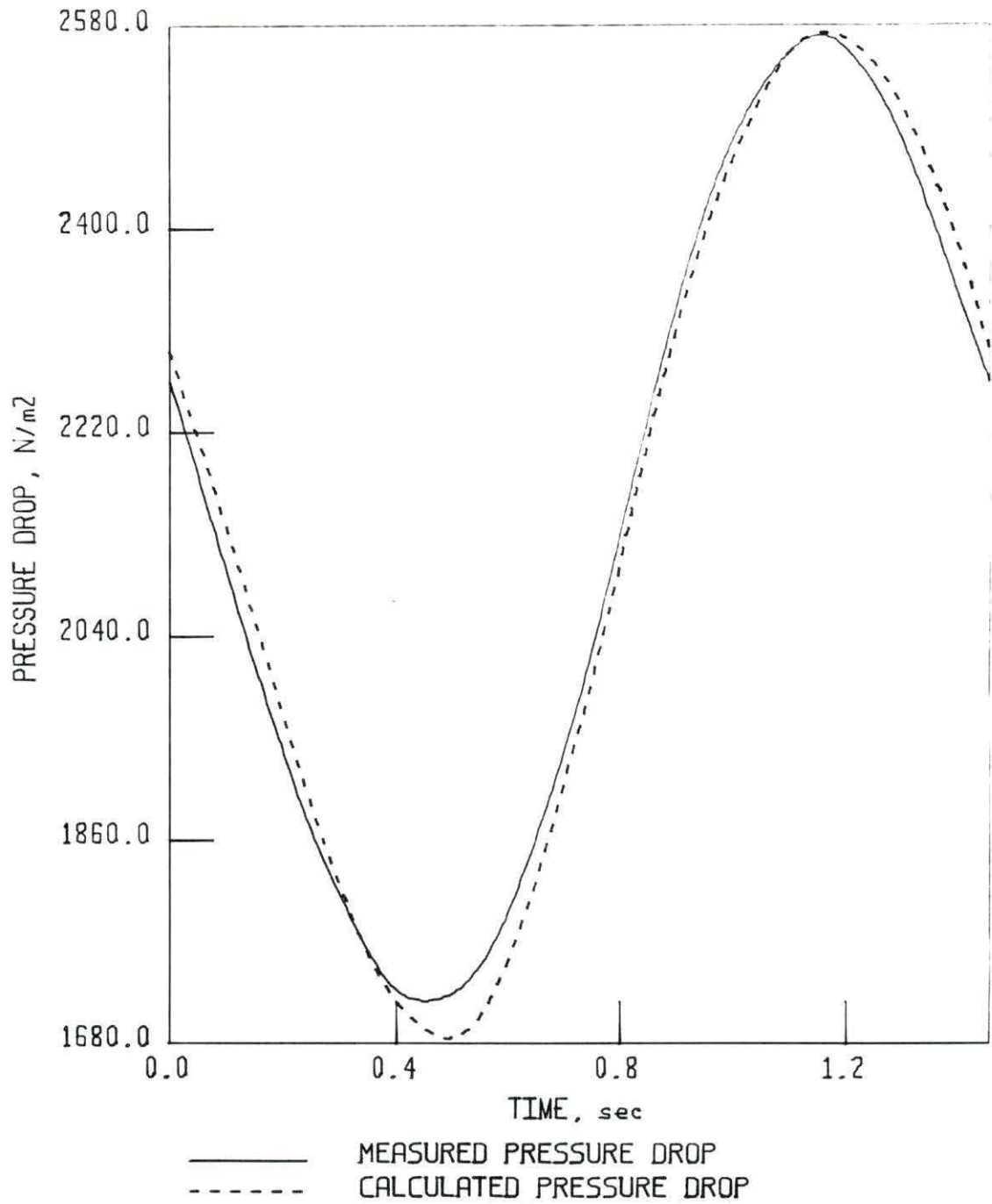


FIGURE 23. Pressure drop waveforms for the 88% stenosis ( $\alpha=6.4$ )

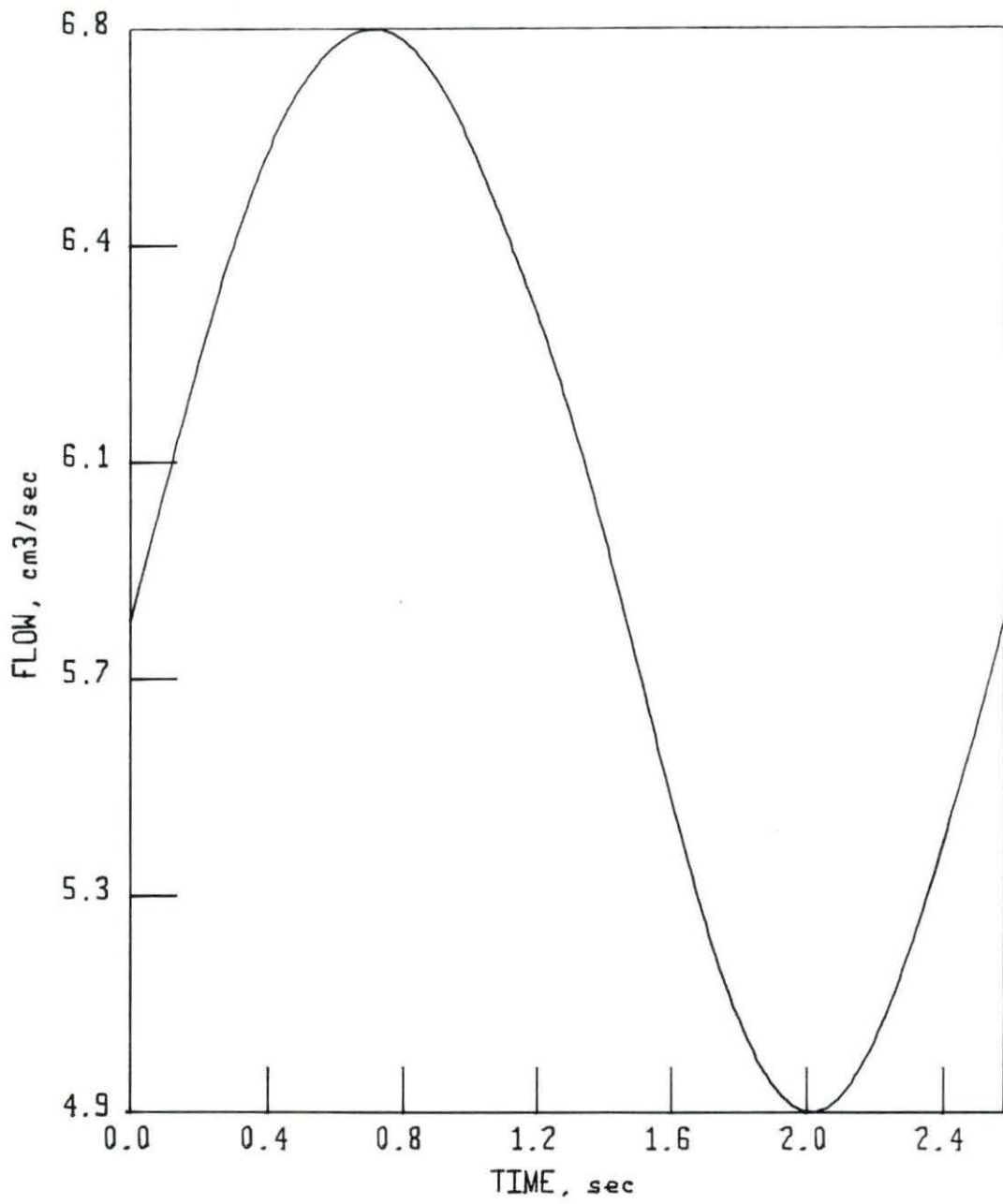


FIGURE 24. Flow waveform for the 74% stenosis ( $a=4.8$ )

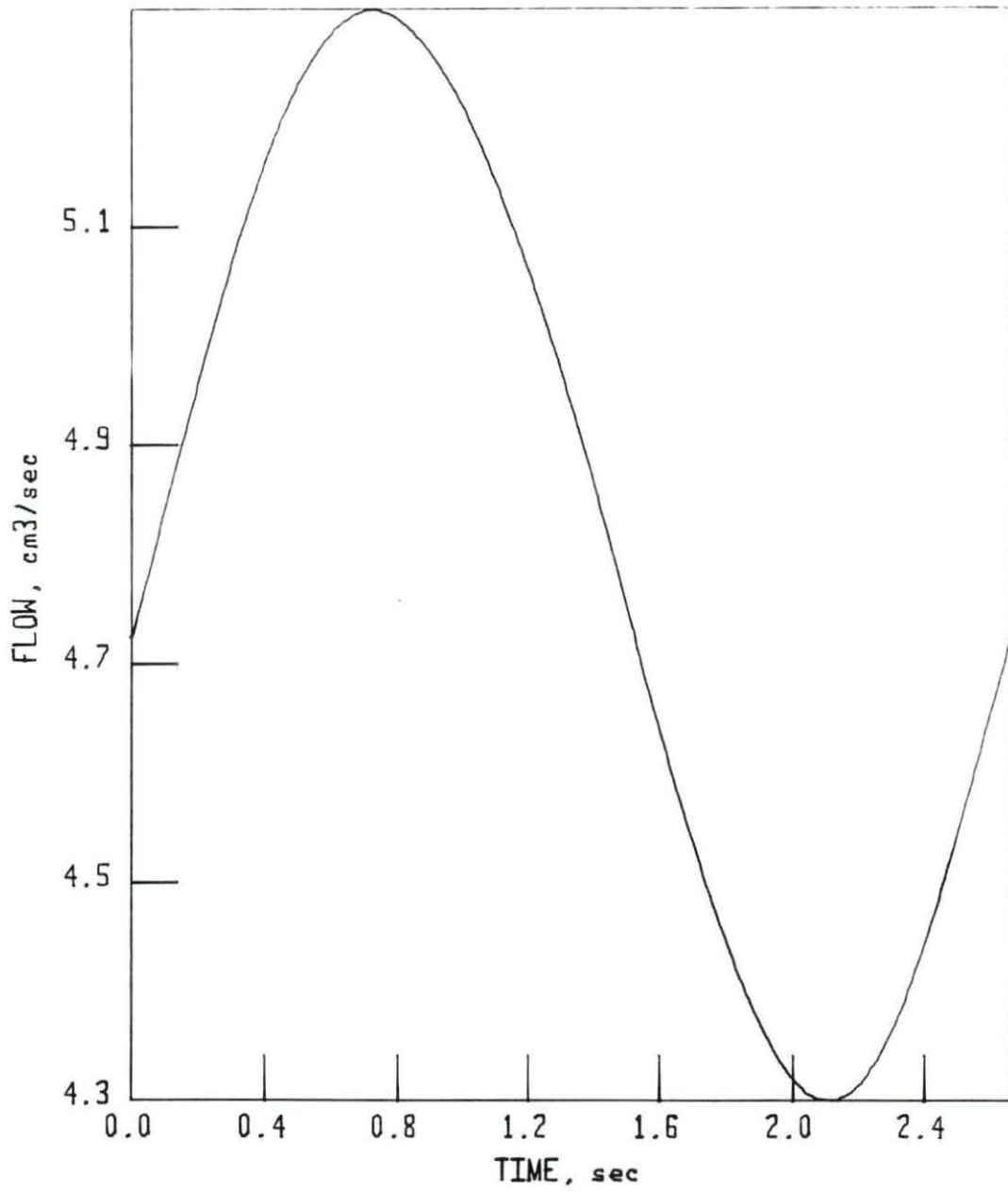


FIGURE 25. Flow waveform for the 82% stenosis ( $a=4.7$ )

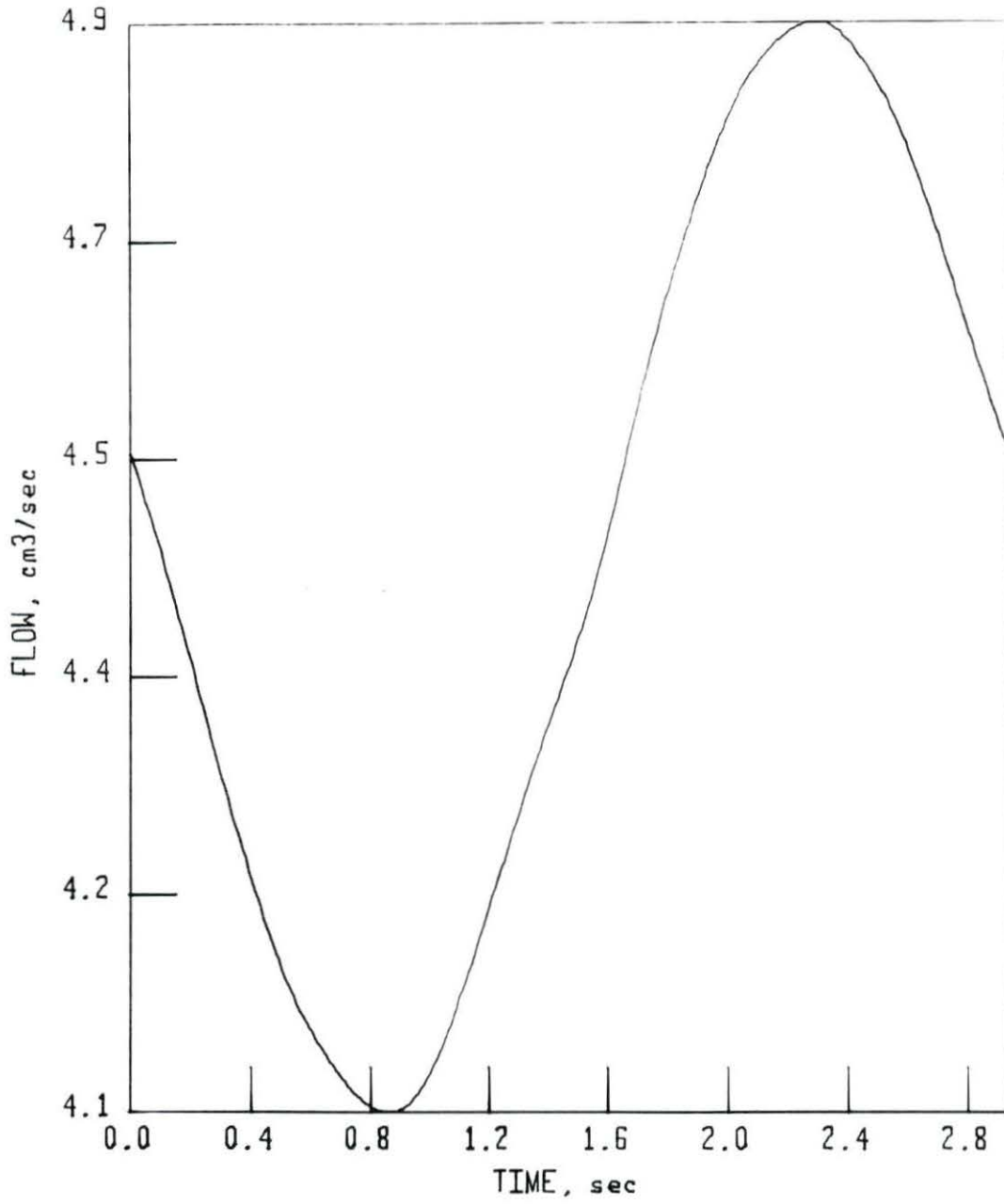


FIGURE 26. Flow waveform for the 88% stenosis ( $a=4.5$ )

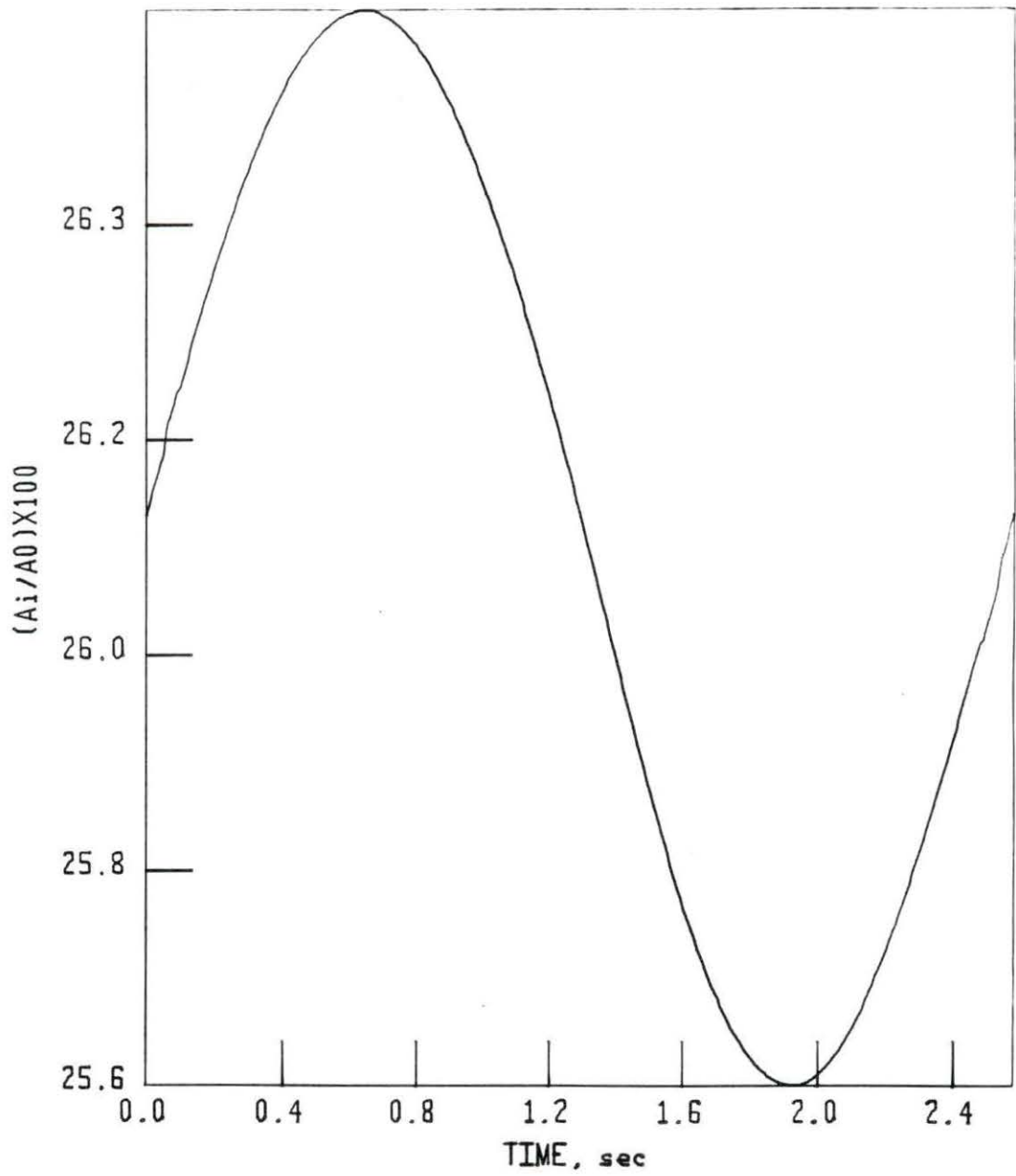


FIGURE 27. Variation in stenosis lumen area for the 74% stenosis ( $\alpha=4.8$ )

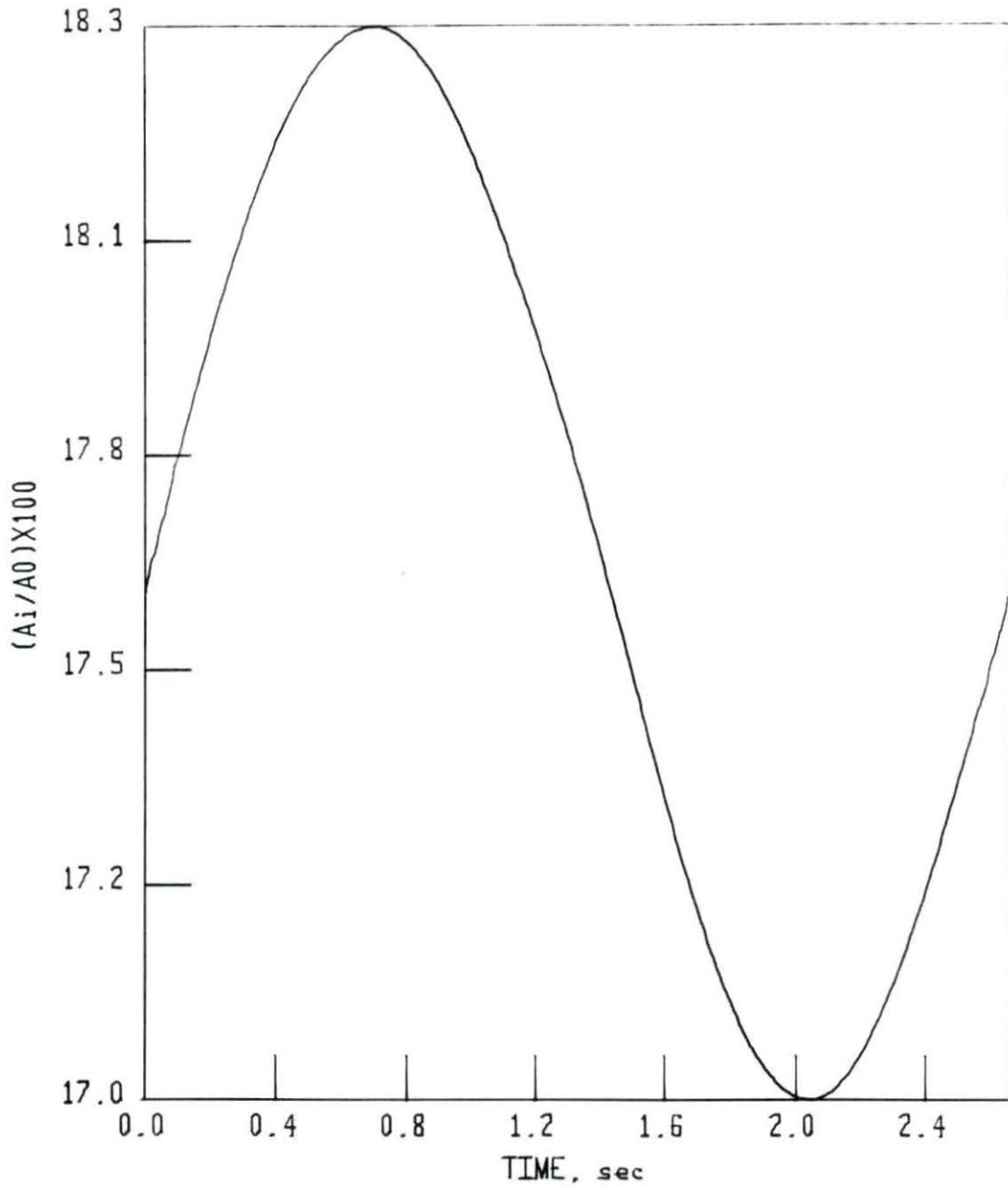


FIGURE 28. Variation in stenosis lumen area for the 82% stenosis ( $a=4.7$ )

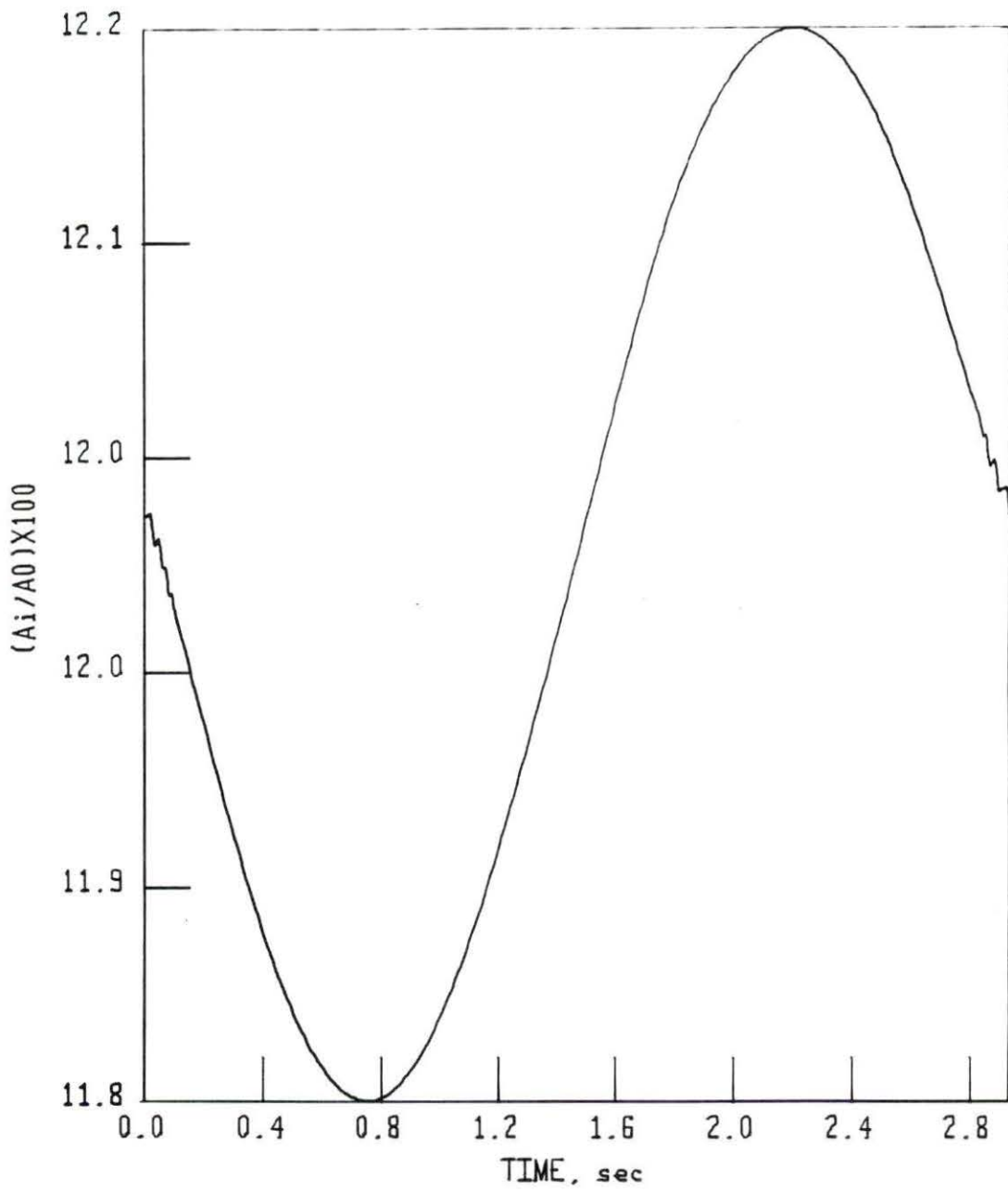


FIGURE 29. Variation in stenosis lumen area for the 88% stenosis ( $a=4.5$ )

stenosis, respectively. The changes in severity of the stenosis (percent area reduction) were relatively small (less than 2% for all stenoses), yet enough to cause significant severity fluctuations, especially for the critical stenoses.

The significance of compliance is shown schematically in Figs. 30-32. In each of the figures, the pressure drop as predicted by the mathematical model, and the pressure drop predicted for zero effective compliance ( $C/A_0 = 0$ ) and mean stenosis severity ( $A_i/A_0 = (A_i/A_0)_{\text{mean}}$ ) were compared. The stenosis with zero effective compliance and mean severity is expected to represent the 'equivalent' rigid stenosis.

From the Figs. 30-32, it is obvious that the pressure drop waveform for the compliant stenosis can be markedly different from that of the equivalent rigid stenosis. The compliant stenosis tends to damp out the extremes of the pressure drop waveform. The mechanism for that is clear, since at high pressures the effective severity of the stenosis drops, whereas at low pressures the effective severity of the stenosis is greater, because the stenosis is narrowed. For rigid stenoses ( $C/A_0 = 0$ ), the effective severity is of course independent of the distending pressure.

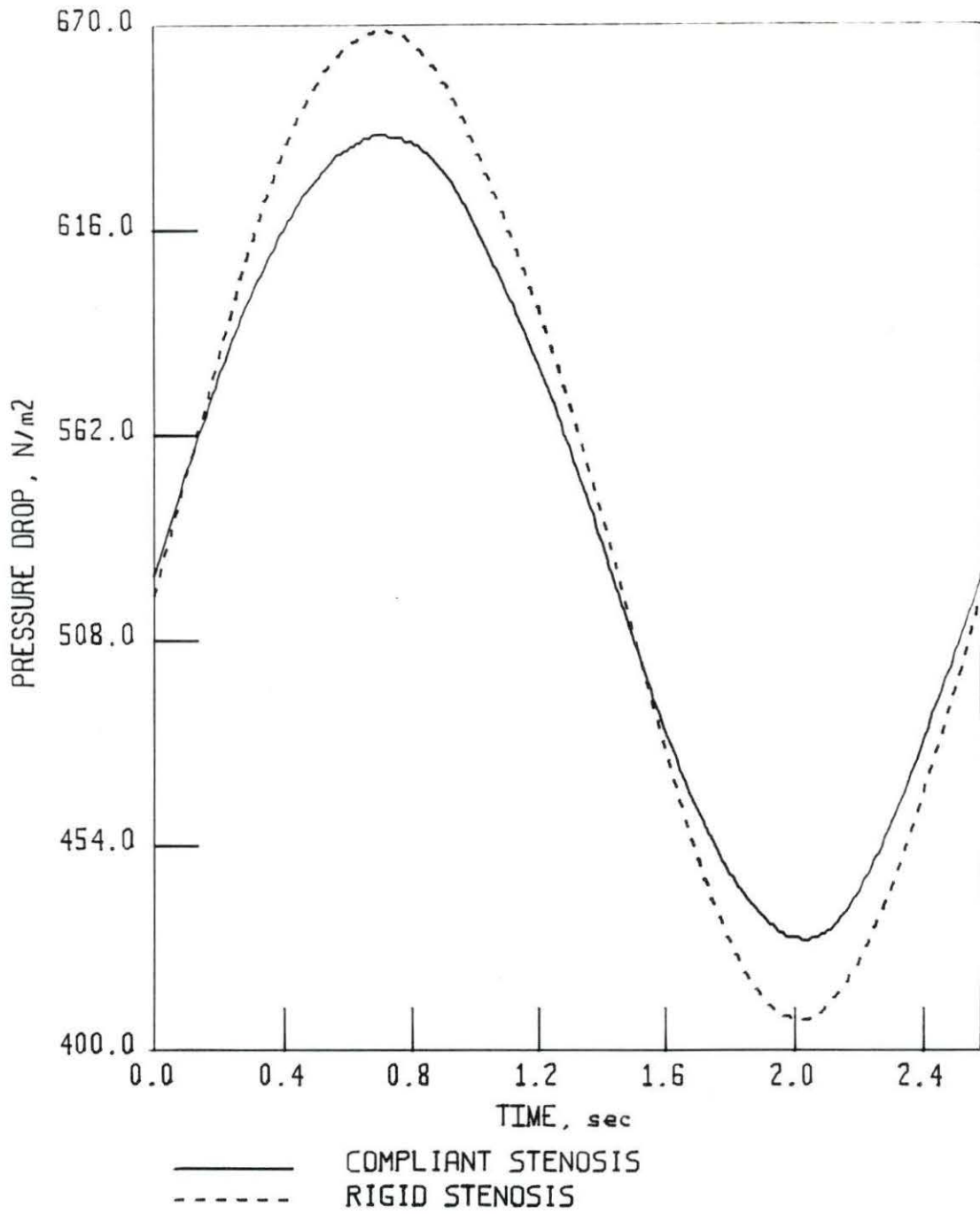


FIGURE 30. Compliant vs rigid 74% stenosis ( $a=4.8$ )

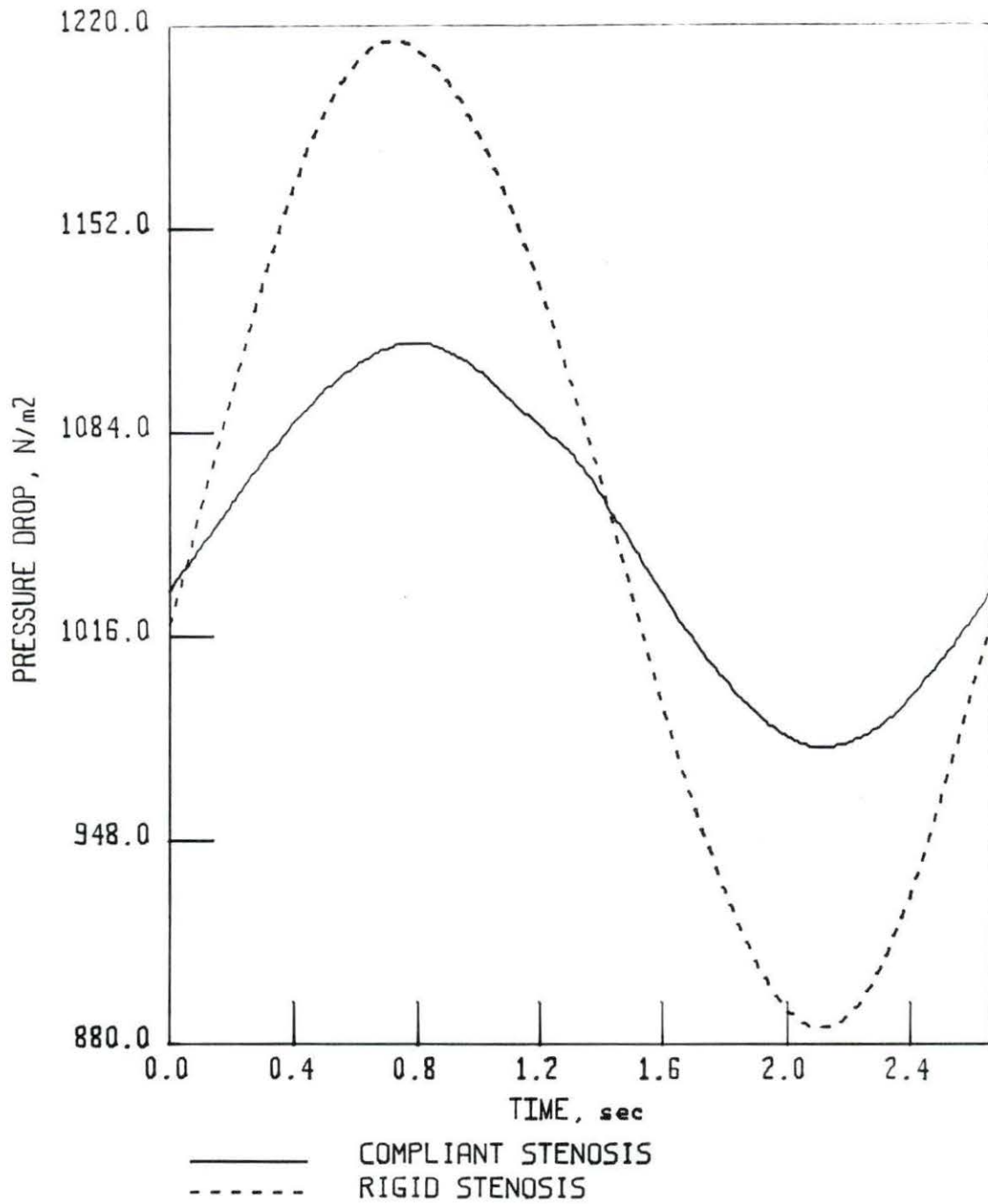


FIGURE 31. Compliant vs rigid 82% stenosis ( $a=4.7$ )

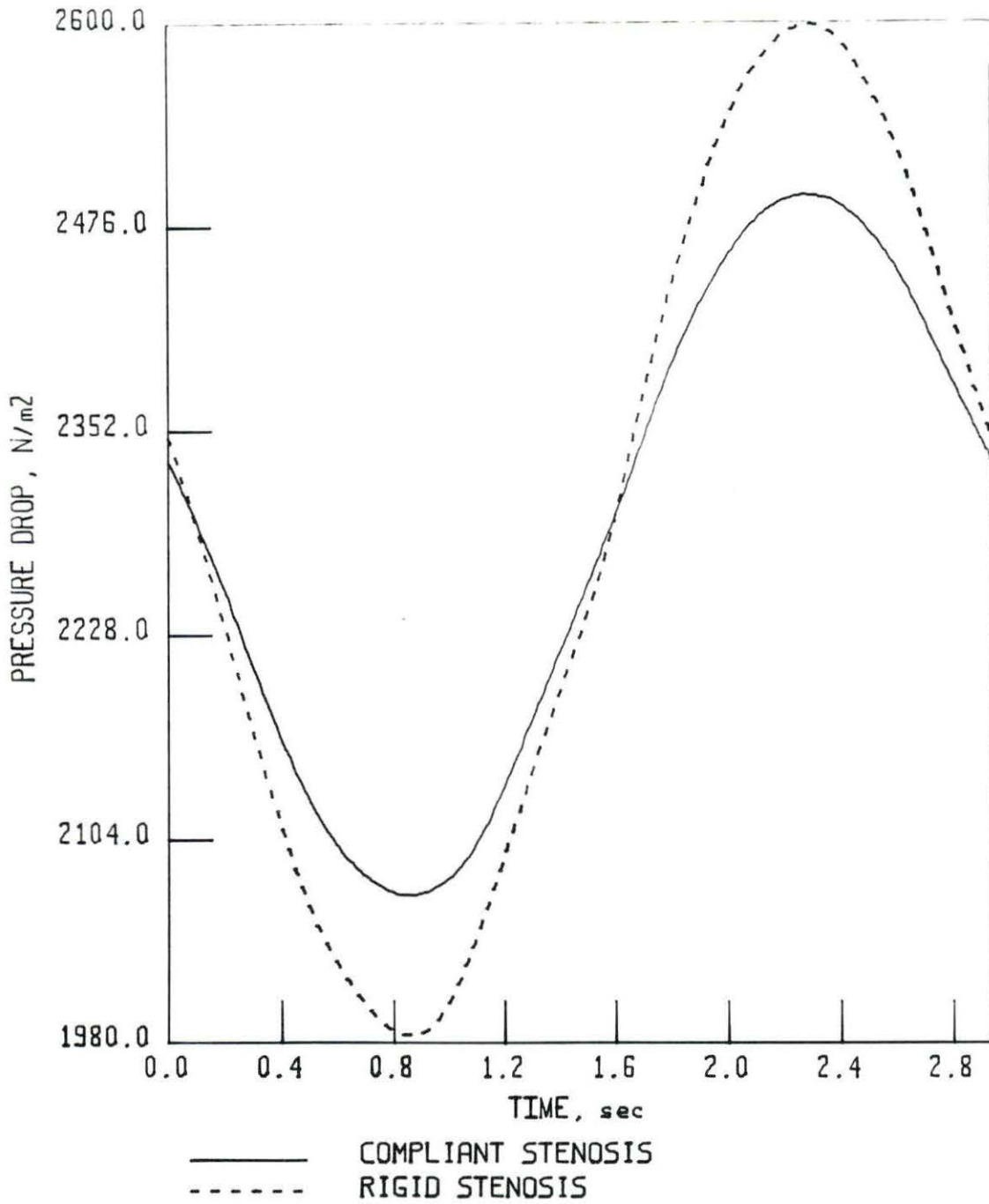


FIGURE 32. Compliant vs rigid 88% stenosis ( $a=4.5$ )

## Interdependence of the Parameters

Dependence of  $\beta$  on  $p^*$ 

The coefficient  $\beta$  exhibited a strong dependence on the selected value of  $p^*$ . The high correlation between the two was the primary reason that not all three coefficients could be simultaneously estimated using statistical procedures. The dependence of  $\beta$  on different values of  $p^*$ , is shown in Table 2.

TABLE 2. Dependence of  $\beta$  on  $p^*$   
( $4.5 < a < 4.8$ )

$p^*$ (cm H <sub>2</sub> O)	$\beta$ values		
	74%	82%	88%
5	3.01	6.67	5.38
15	2.78	5.40	4.78
25	2.52	4.21	4.13
35	2.22	3.08	3.43
45	1.87	1.99	2.66

Dependence of effective compliance on  $p^*$ 

The effective compliance is not strongly dependent on  $p^*$ . Assuming different values of  $p^*$ , the estimated values of  $C/A_0$  for the same set of data were relatively close to each other suggesting that the correlation between  $p^*$  and  $C/A_0$  is small. Table 3 summarizes these findings.

TABLE 3. Dependence of  $C/A_0$  on  $p^*$   
( $4.5 < a < 4.8$ )

$p^*$ (cm H <sub>2</sub> O)	$C/A_0$ values ( $\times 10^5$ m <sup>2</sup> /N)		
	74%	82%	88%
5	0.49	1.43	0.51
15	0.53	1.43	0.53
25	0.56	1.44	0.56
35	0.62	1.46	0.60
45	0.67	1.49	0.65

#### Stenosis in Collapsing Mode

As mentioned earlier, some exploratory pulsating flow tests for stenoses in the collapsed mode were run for all three stenoses. During the tests the tube was either collapsed throughout the cycle, or it was in a collapsing mode for part of the cycle. Collapsing, which was induced by decreasing the distal resistance, was determined 'by eye'. The tube was considered to be in collapsed mode when its cross-sectional geometry changed radically, going from an approximately circular cross-section to a flat, strip-like appearance. Collapsing always occurred downstream of the stenosis, starting usually at most distal part of the elastic tubing.

The results of the collapsed mode experiments are shown schematically in figures 33-38. In figures 33, 35, and 37, the proximal pressure,  $p_1(t)$  and the flow,  $Q(t)$ , waveforms were drawn normalized to the same scale (by multiplying the flow waveform by a constant and adding a constant, so that the peak and bottom points of the two curves match), for better comparison. Figures 34, 36, and 38 are supplementary to the first three ones in a sense that the distal pressure,  $p_2(t)$ , is plotted on scale with the proximal pressure,  $p_1(t)$ , so that the behavior of the distal pressure over the cycle is more clearly seen.

Examining the figures the following major conclusions can be drawn:

- When the tube is in collapsed mode, the distal pressure drops at low levels and remains practically constant over the cycle. This behavior of the distal pressure can be viewed better in Fig. 34 for the 74% stenosis where for part of the cycle (left side of the graph), the tube is in uncollapsed (open) mode, and for the remainder of the cycle (right side of the graph), it is in a collapsed mode. When the tube changes from the collapsed to uncollapsed mode, the distal pressure rises sharply from very low values (in the

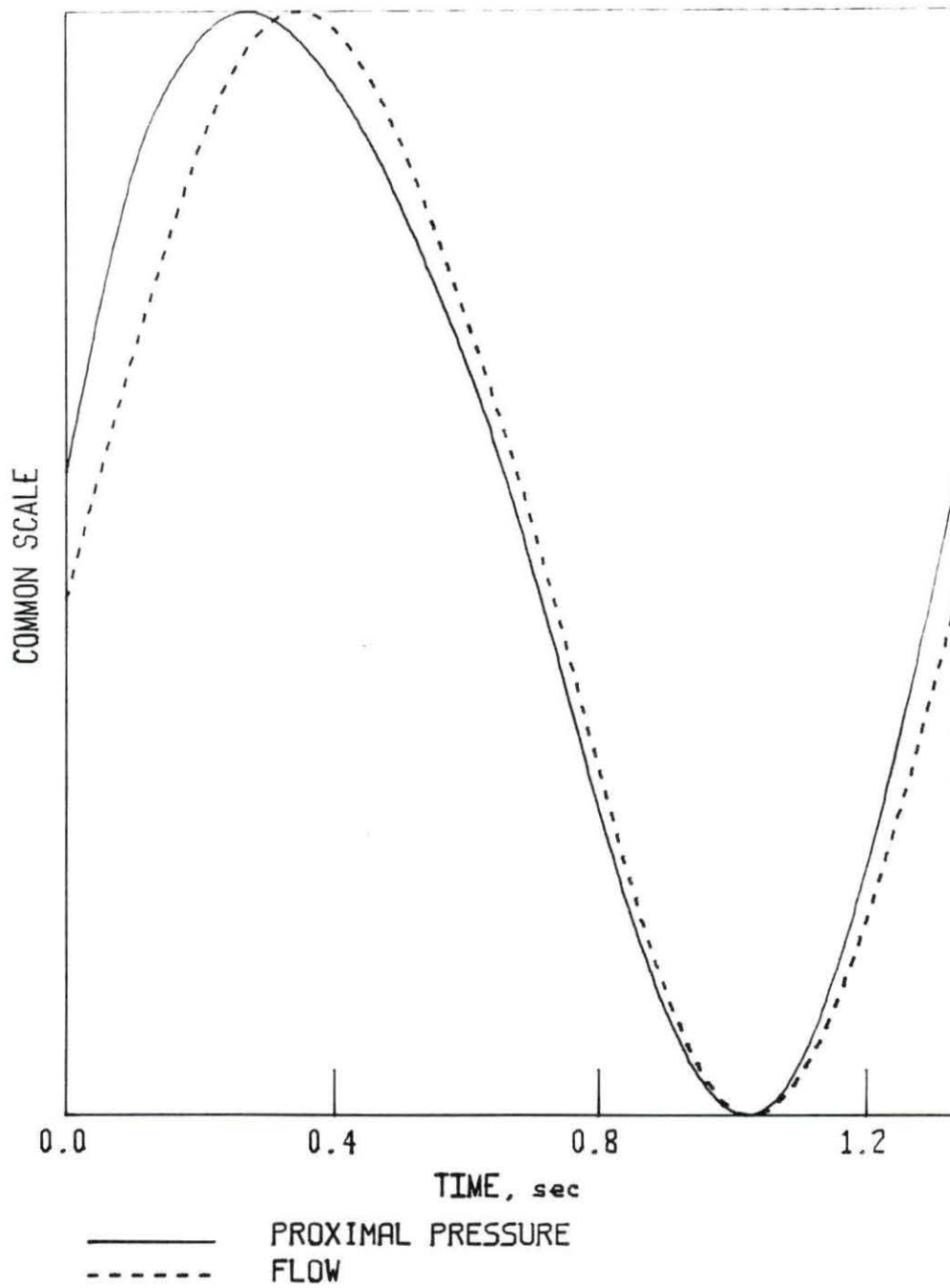


FIGURE 33. Pressure and flow waveforms for the 74% stenosis in collapsed mode ( $a=4.8$ )

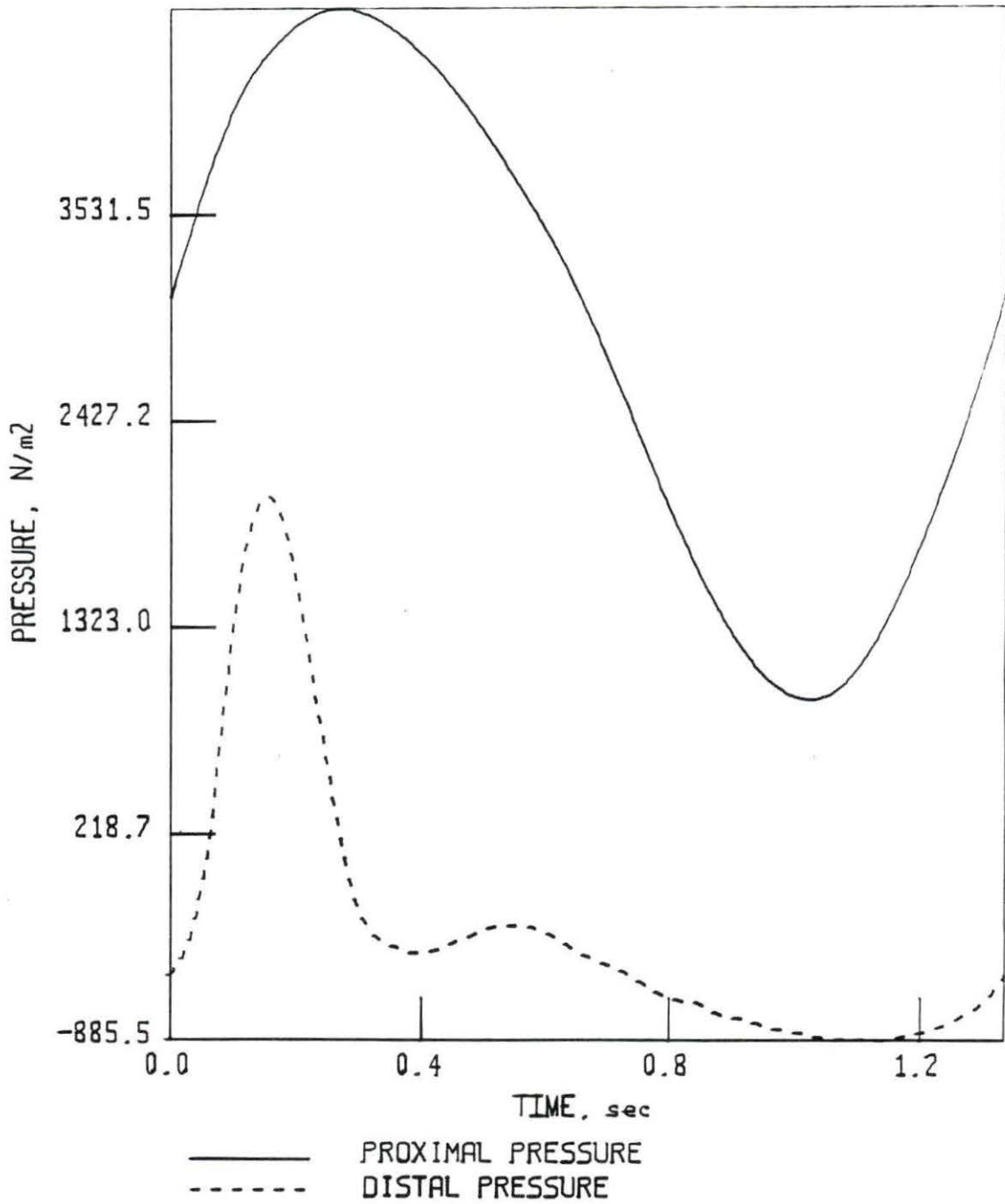


FIGURE 34. Proximal and distal pressure waveforms for the 74% stenosis in collapsed mode ( $\alpha=4.8$ )

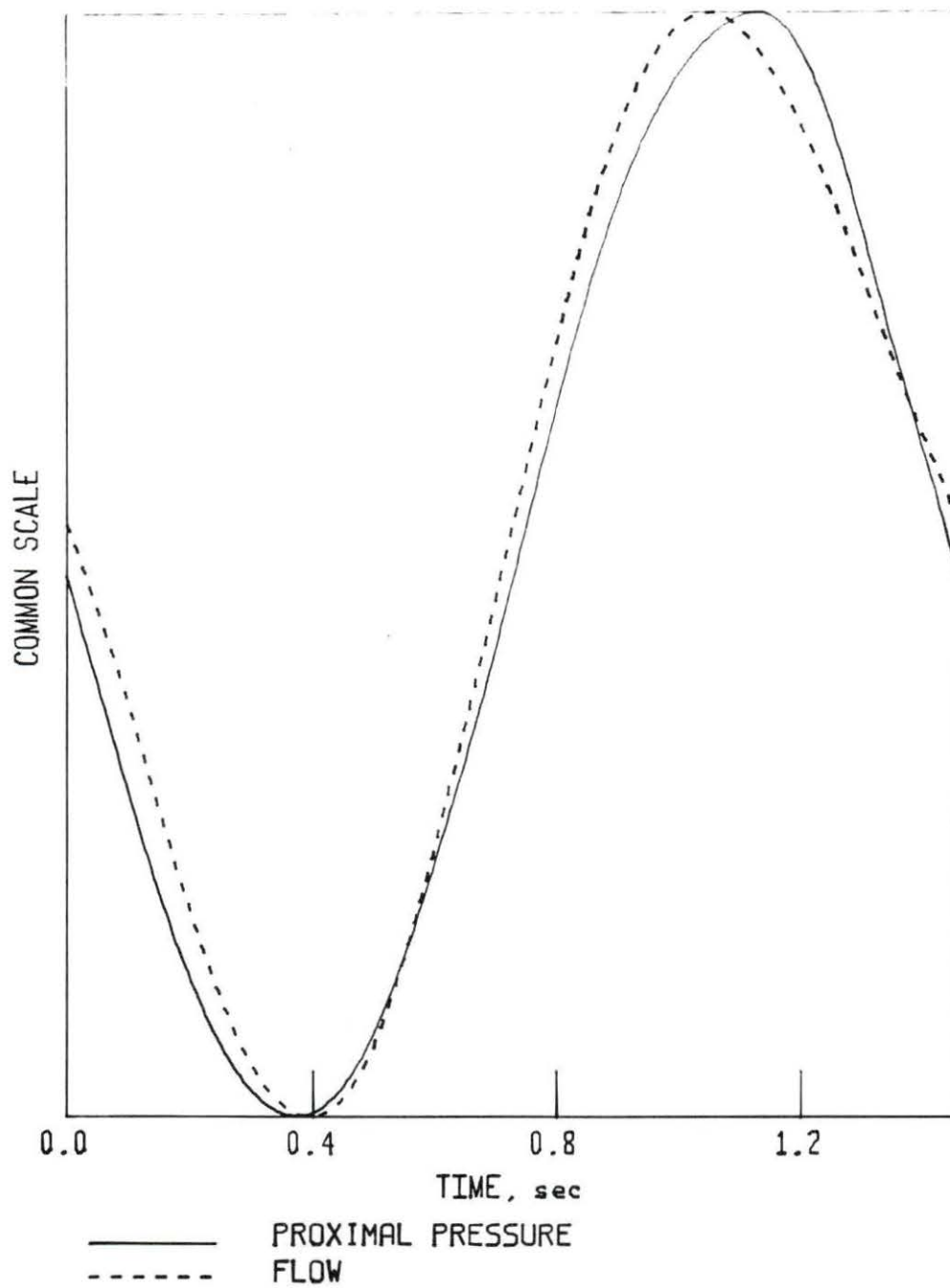


FIGURE 35. Pressure and flow waveforms for the 82% stenosis in collapsed mode ( $a=4.7$ )

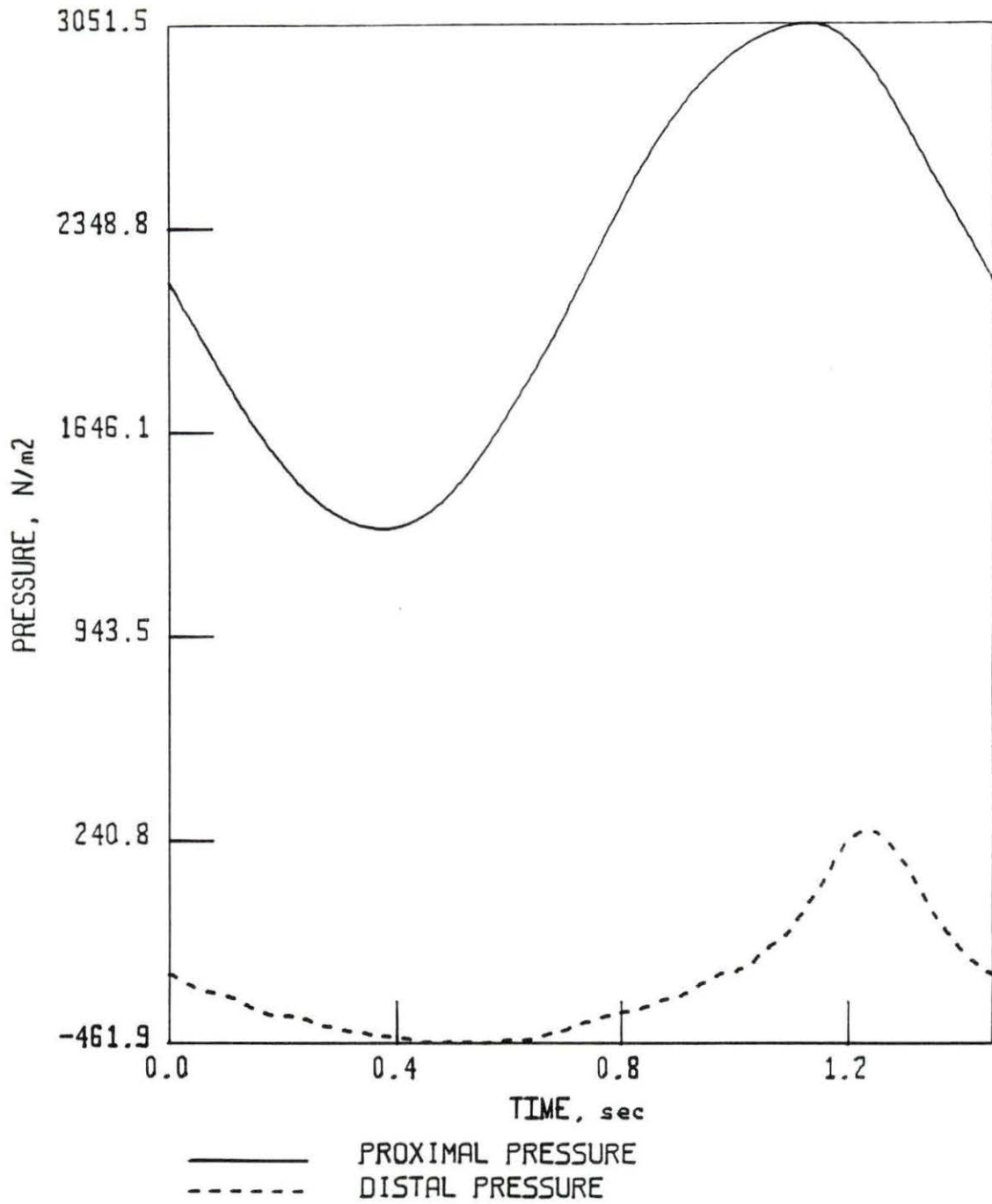


FIGURE 36. Proximal and distal pressure waveforms for the 82% stenosis in collapsed mode ( $\alpha=4.7$ )

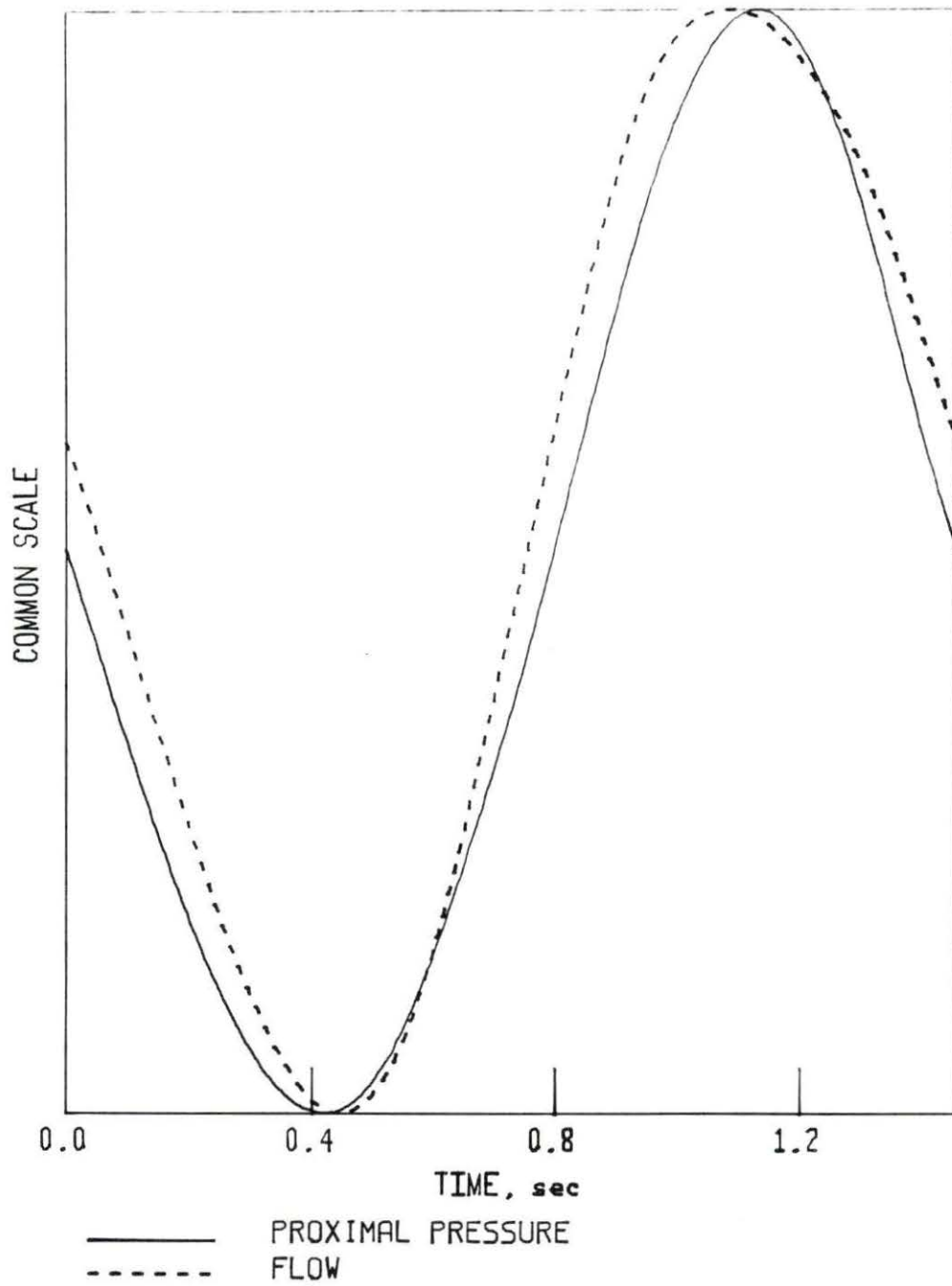


FIGURE 37. Pressure and flow waveforms for the 88% stenosis in collapsed mode ( $a=4.5$ )

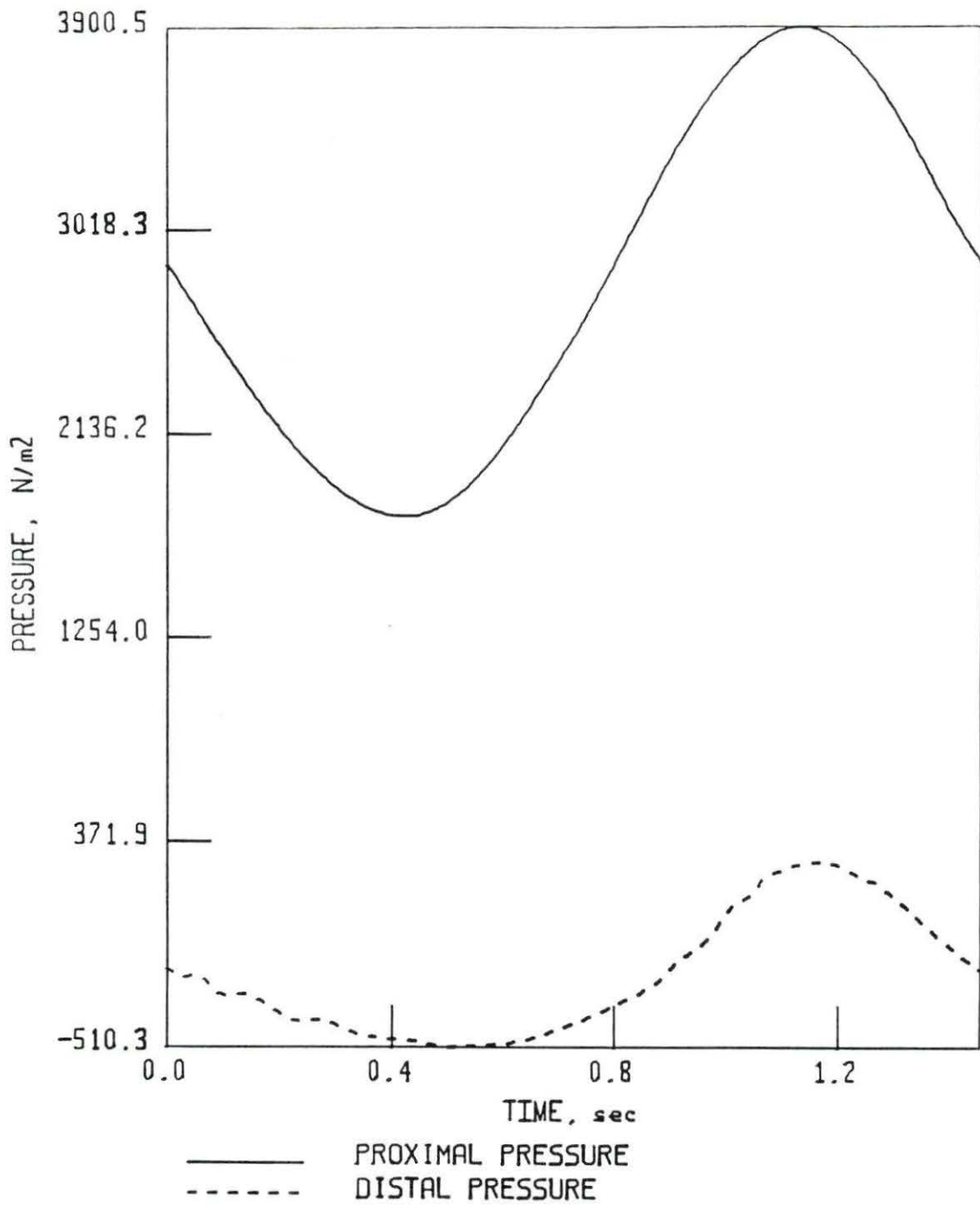


FIGURE 38. Proximal and distal pressure waveforms for the 88% stenosis in collapsed mode ( $a=4.5$ )

neighborhood of zero or less) to high values (2000  $\text{N/m}^2$ ), comparable to those in the fully uncollapsed mode experiments and of the same order of magnitude as the proximal pressure values. In contrast, when the tube is in a collapsed mode, the values of the distal pressure remain at low levels without exhibiting significant oscillation, thus being approximately independent of the changes in flow,  $Q(t)$ , and the proximal pressure,  $p_1(t)$ . The same situation holds for the 82% and the 88% stenosis cases, where the tube was in collapsed mode throughout the cycle, as seen in Figs. 36 and 38.

- When the stenosis was in collapsed mode, the flow waveform seemed to follow closely the proximal pressure waveform. As a consequence, the flow waveform follows the changes in the pressure drop waveform,  $p_1(t) - p_2(t)$ , since, as mentioned earlier, in the collapsing case  $p_2(t)$  remains practically constant. This phenomenon is demonstrated in all Figs. 33, 35, and 37; moreover, Fig. 33 shows nicely the striking differences between the two states: on the right side of the graph, where the tube is collapsed, the two curves ( $Q$  and  $p_1$ ) are almost identical in shape; on the left side of the

graph, where the tube is in uncollapsing mode, the two curves behaved in a more independent fashion.

- When the stenoses were in a collapsed mode, the pressure drop across the stenotic and collapsed segment did not differ significantly between the three stenoses. In contrast to the case of uncollapsed stenotic flow where the difference of the mean pressure drop between the subcritical (74%) and the critical (88%) stenosis was great, in the collapsed mode the differences were small. The apparent cause of this difference in behavior is that in the collapsed state, a great part of the pressure drop across the collapsed-stenosed segment is due to the increased resistance of the collapsed segment downstream of the stenosis, which is common and acts essentially identically for all three stenoses.

## SUMMARY AND CONCLUSIONS

The results of this study indicates that the theoretical model developed for the uncollapsing case can be used to adequately describe the pulsatile flow in compliant stenoses. The incorporation of the compliance in the already existing models for rigid stenoses was successful and proved to be a necessary improvement for a better description of the flow. On the other hand, the results of the experiments on pulsatile flow through collapsed compliant stenoses demonstrated some of the main differences between the two flow situations. The results reconfirmed and extended, at least in a qualitative fashion, some of the previous findings of studies on collapsing tubes, for the general case of pulsatile flow.

Using the estimated values for  $\beta$  and  $C/A_0$ , the model was able to fit the experimental data well, for all alpha values and for all three stenoses. From the application of the theoretical model to the experimental data, for the case of an uncollapsed tube, the following major conclusions were drawn:

- The inertial forces can be neglected without introducing significant error even for the mildest (74% area reduction) of the stenoses.

- The simplified pressure-area relationship used in the model was satisfactory in taking into account the stenosis compliance.
- There was a significant correlation between the reference pressure,  $p^*$ , and the correction factor,  $\beta$ ; and because of this strong correlation, both  $p^*$  and  $\beta$  could not be determined simultaneously using statistical procedures. In general,  $\beta$  was sensitive to very small changes in  $p^*$ .
- The effective compliance,  $C/A_0$ , showed little dependence on the  $p^*$  values, and minimal dependence on the alpha parameter. The estimated values for the effective compliance,  $C/A_0$ , however, differed between stenoses. The differences can be attributed partly to the different structural support for different percent stenoses, and also to the probable small differences in the elastic properties of the tubing used. The question as to whether the estimated effective compliances have any physical meaning, as well as the explanation for the large deviations between estimated compliances (although the estimation procedure was very stable), was not answered in this study.

- For the critical stenoses (82% and 88%),  $\beta$  exhibited a slight dependence on the pulsatility of flow and always decreased when  $a$  increased. Although the explanation for this trend is not clear, it is anticipated that the entrance-exit effects that  $\beta$  accounts for, are somehow decreased by the increased unsteadiness of the flow.
- The subcritical, yet severe 74% stenosis, behaved differently than the critical ones, as far as pulsatility is concerned. At low alpha values ( $a = 4.8$ ),  $\beta$  was 3.52 and the effective compliance,  $C/A_0$ , was  $0.57 \times 10^{-5} \text{ m}^2/\text{N}$ . These values are close to those found for the critical stenoses. However, at high alpha values ( $a > 5.5$ ),  $\beta$  was approximately equal to one and the effective compliance was practically zero ( $C/A_0 < 10^{-7}$ ).

From the evaluation of the exploratory experimental data obtained in the collapsing mode experiments, the following major conclusions are drawn:

- In the collapsed state the flow rate,  $Q(t)$ , follows closely the proximal pressure. This observation supports the previous findings based on steady flow tests in stenosed and unstenosed compliant tubes (i.e., Lopez-Muniz et al. 1968; Dubill 1986), where

the following pressure-flow relationship was proposed:

$$Q = k(p_1 - p_e)$$

$p_e$  being the external pressure, and  $k$  be a constant.

- In the collapsed state, the pressure distal to the collapsed segment drops to low levels and remains practically constant over the cycle, showing minimal dependence on the flow and proximal pressure waveforms.
- When in a collapsed state, the effective hydrodynamic severity of the stenotic segment increases significantly, compared to the uncollapsed state. This is because the increase in severity is due both to the reduction in the cross-sectional area on the elastic tube distal to stenosis and in the stenosis itself. Thus, in collapsed tubes, the distinction between critical and subcritical stenosis is not clear.

Direct clinical implications from the present study cannot be easily made, mainly because the type of flow and model stenosis used are simple idealizations of blood flow through compliant arterial stenoses. The study, however, emphasizes some important points with medical or clinical implications. First, for pulsatile flow through compliant

stenoses, the stenosis behaves in a dynamic fashion. It alters its geometric characteristics over the pulsating cycle, which leads to a damped pressure drop waveform, that is different from that of a rigid stenosis. Second, in order to model pulsatile flow through compliant stenoses, it is very important that a good knowledge of the geometrical characteristics, as well as the elastic properties of the compliant portion of the arterial wall, is achieved.

As far as modeling blood flow in arteries is concerned, the findings of this study suggest that the stenotic segment along with the distal portion of the artery subject to collapsing should be treated as a unique element. In the uncollapsed (open-tube) state, good estimates of the three parameters  $p^*$ ,  $\beta$ , and  $C/A_0$  are essential to describe the flow. Knowledge of the  $p^*$  value is important because  $p^*$  relates to a specific geometry of the stenotic segment, thus giving a reference starting point for the theoretical model. The high correlation between  $p^*$  and  $\beta$  does not allow for the simultaneous estimation of the two, so that for any parameter estimation procedure to be applied, one of the two should be somehow specified. For the case of a fully collapsed vessel (artery), flow is directly related to the proximal pressure and essentially independent of the distal pressure. Although an exact relationship was not

established in this study for the collapsed case, the fact that the inertial forces proved to be totally insignificant for all stenosis severities studied suggests that models developed for the steady flow case may be appropriate for pulsatile flows simulating blood flow in arteries.

It is recommended that additional studies on the mechanical (elastic) properties of the compliant stenosis be carried out to provide the necessary background for future studies on the fluid mechanics of compliant stenoses. In vivo studies should also be performed to evaluate the findings of the present study for the complex geometries and flows existing in the circulation. As a continuation of this study, and because of its major clinical interest, additional work involving the study of pulsating flow in collapsed compliant stenoses should be undertaken.

## BIBLIOGRAPHY

- Brower, Robert W., and Abraham Noordergraaf. 1973. Pressure-Flow Characteristics of Collapsible Tubes: A Reconciliation of Seemingly Contradictory Results. *Annals of Biomedical Engineering* 1:333-355.
- Brown, B. Greg, Bolson, Edward L., and Harold T. Dodge. 1984. Dynamic Mechanisms in Human Coronary Stenosis. *Circulation* 70(6):917-922.
- Caro, C. G., Pedley, T. J., Schroter, R. C., and W. A. Seed. 1978. *The Mechanics of the Circulation*. Oxford University Press, Oxford, England.
- Conrad, William A. 1969. Pressure-Flow Relationships in Collapsible Tubes. *IEEE Transactions on Biomedical Engineering* BME-16(4):284-295.
- Dubill, Patricia M. 1986. Steady Flow Through Models of Compliant Stenoses. M.S. thesis. Iowa State University, Ames, Iowa.
- Elliott, E. A., and S. V. Dawson. 1978. Fluid Velocity Greater than Wavespeed and the Transition from Supercritical to Subcritical Flow in Elastic Tubes. *Medical and Biological Engineering and Computing* 17:192-198.
- Forrester, J. H., and D. F. Young. 1970. Flow Through a Converging-Diverging Tube and its Implications in Occlusive Vascular Disease. *Journal of Biomechanics* 3:303-316.
- Freudenburg, H., and P. R. Lichtlen. 1981. The Normal Wall Segment in Coronary Stenosis--A Postmortem Study. *Zeitschrift fuer Kardiologie* 70:863-869.
- Fry, Donald L. 1959. Measurement of Pulsatile Flow by the Computed Pressure Gradient Technique. *IRE Transactions of Medical Electronics* ME-6:259-264.
- Fry, Donald L., Thomas, Lewis J., and Joseph C. Greenfield, Jr. 1980. Flow in Collapsible Tubes. Pages 407-424 in Dali J. Patel and Ramesh N. Vaishnav, eds. *Basic Hemodynamics and its Role in Disease Processes*. University Park Press, Baltimore, Maryland.

- Greenfield, J. C., Jr., and D. L. Fry. 1965. Relationship between instantaneous aortic flow and the pressure gradient. *Circulation Research* 17:340-348.
- Gould, K. Lance. 1978. Pressure-Flow Characteristics of Coronary Stenoses in Unsedated Dogs at Rest and During Coronary Vasodilation. *Circulation Research* 43(2):242-253.
- Holmberg, J. L., and T. A. Wilson. 1970. Mechanics of the Flow in an Elastic Tube Extending from an Orifice into a Pressure Vessel. *Journal of Applied Mechanics* 70-APM-ZZ:1-5.
- Lee, J. S., and Y. C. Fung. 1970. Flow in Locally Constricted Tubes at Low Reynolds Numbers. *ASME Journal of Applied Mechanics* 37:9-16.
- Lipscomb, Kirk, and Steven Hooten. 1978. Effect of Stenotic Dimensions and Blood Flow on the Hemodynamic Significance of Model Coronary Arterial Stenoses. *The American Journal of Cardiology* 42:781-792.
- Logan, Samuel E. 1975. On the Fluid Mechanics of Human Coronary Artery Stenosis. *IEEE Transactions on Biomedical Engineering* BME-22(4):327-334.
- Lopez-Muniz, R., Stephens, N. L., Bromberger-Barnea, B., Permutt, S., and R. L. Riley. 1968. Critical Closure of Pulmonary Vessels Analyzed in Terms of Starling Resistor Model. *Journal of Applied Physiology* 24:625-635.
- McDonald, D. A. 1974. *Blood Flow in Arteries*. Williams and Wilkins Co., Baltimore, Maryland.
- Maseri, A., Severi, S., DeNes, M., L'Abbate, A., Chierchia, S., Marzilli, M., Ballestra, A. M., Parodi, O., and A. Distante. 1978. "Variant" Angina. One Aspect of a Continuous Spectrum of Vasospastic Myocardial Ischemia: Pathogenic Mechanisms, Estimated Incidence, Clinical and Arteriographic Findings in 138 Patients. *American Journal of Cardiology* 42:1019-1078.
- Milnor, William R. 1982. *Hemodynamics*. Waverly Press, Inc., Baltimore, Maryland.
- Morgan, B. E., and D. F. Young. 1974. An Integral Method for the Analysis of Flow in Arterial Stenosis. *Bulletin of Mathematical Biology* 36:39-53.

- Rodbard, Simon. 1955. Flow Through Collapsible Tubes: Augmented Flow Produced by Resistance at the Outlet. *Circulation* 11:280-287.
- Rodbard, Simon, and Hiroshi Saiki. 1953. Flow Through Collapsible Tubes. *American Heart Journal* 46:715-725.
- Rubinow, S. I., and Joseph B. Keller. 1972. Flow of a Viscous Fluid Through an Elastic Tube with Applications to Blood Flow. *Journal of Theoretical Biology* 35:299-313.
- Santamore, William P. 1986. Models of Vasospasm: Relation of Organic Stenosis to Sites of Vasospasm. Pages 363-371 in *Arterial Diseases: Atherosclerosis, Hypertension, and Vasospasm*. Alan R. Liss, Inc., Baltimore, Maryland.
- Santamore, William P., and Alfred A. Bove. 1985. A Theoretical Model for the Compliant Stenosis. *American Journal of Physiology* 248:H274-H286.
- Santamore, William P., and Paul Walinsky. 1980. Altered Coronary Flow Responses to Vasoactive Drugs in the Presence of Coronary Arterial Stenosis in the Dog. *The American Journal of Cardiology* 45:276-285.
- Santamore, William P., Walinsky, Paul, Bove, Alfred A., Cox, Robert H., Carey, Rita A., and James F. Spann. 1980. The Effects of Vasoconstriction on Experimental Coronary Artery Stenosis. *American Heart Journal* 100(6):852-858.
- Santamore, William P., Bove, Alfred A., Carey, Rita, Walinsky, Paul, and James F. Spann. 1981. Synergistic Relation between Vasoconstriction and Fixed Epicardial Vessel Stenosis in Coronary Artery Disease. *American Journal of Cardiology* 43:219-224.
- Schonfeld, J. C. 1949. Resistance and Inertia of the Flow of Liquids in a Tube or Open Canal. *Applied Scientific Research* A1:169-197.
- Schwartz, Jeffrey S., Carlyle, Peter F., and Jay N. Cohn. 1979. Effect of Dilation of the Distal Coronary Bed on Flow and Resistance in Severely Stenotic Coronary Arteries in the Dog. *The American Journal of Cardiology* 43:219-224.
- Schwartz, Jeffrey S., Carlyle, Peter F., and Jay N. Cohn. 1980. Effect of Coronary Arterial Pressure on Coronary Stenosis Resistance. *Circulation* 61(1):70-76.

- Seeley, B. D., and D. F. Young. 1976. Effect of Geometry on Pressure Losses Across Models of Arterial Stenosis. *Journal of Biomechanics* 9:439-448.
- Shapiro, Ascher H. 1977. Steady Flow in Collapsible Tubes. *Journal of Biomechanical Engineering* 99:126-147.
- Uchida, S. 1956. The Pulsating Viscous Flow Superposed on the Steady Laminar Motion of Incompressible Fluid in a Circular Pipe. *ZAMP* 7:403-422.
- Weast, Robert C. 1976. *Handbook of Chemistry and Physics*. 57th ed. CRC Press, Inc., Cleveland, Ohio.
- Womersley, J. R. 1955a. Method for the Calculation of Velocity, Rate of Flow and Viscous Drag in Arteries when the Pressure Gradient is known. *Journal of Physiology* 127:553-563.
- Womersley, J. R. 1955b. Oscillatory Motion of a Viscous Liquid in a Thin-Walled Elastic Tube. I. The Linear Approximation for Long Waves. *Philosophical Magazine* 46:199-221.
- Womersley, J. R. 1957. The Mathematical Analysis of the Arterial Circulation in a State of Oscillatory Motion. Wright Air Development Center, Technical Report WADC-TR56-614.
- Young, D. F. 1968. Effect of a Time-Dependent Stenosis on Flow Through a Tube. *ASME Journal of Engineering for Industry* 90:248-254.
- Young, D. F. 1979. Fluid Mechanics of Arterial Stenoses. *Journal of Biomechanical Engineering* 101:157-175.
- Young, D. F., and F. Y. Tsai. 1973a. Flow Characteristics in Models of Arterial Stenoses - I. Steady Flow. *Journal of Biomechanics* 6:395-410.
- Young, D. F., and F. Y. Tsai. 1973b. Flow Characteristics in Models of Arterial Stenoses - II. Unsteady Flow. *Journal of Biomechanics* 6:547-559.
- Young, D. F., Cholvin, N. R., and A. C. Roth. 1975. Pressure Drop Across Artificially Induced Stenoses in the Femoral Arteries of Dogs. *Circulation Research* 36:735-743.

## ACKNOWLEDGMENTS

I would like to express my sincere appreciation and gratitude to Dr. Donald F. Young for his guidance and support at every stage of this research. Special thanks are rendered to Dr. David Carlson, Dr. Theodore Okiishi, and Dr. Thomas Rogge for serving on the program of study committee. My appreciation is also extended to all faculty, staff, and graduate students of the Biomedical Engineering Program for their valuable suggestions and assistance.

This work is dedicated to the very special people who have supported me along the way: My parents Kostas and Vasiliki Stergiopoulos, for the values instilled and the unending moral support, my brother Vagos, for his joyful spirit, and especially Soula, for her continuous encouragement and love.

## APPENDIX

In this section the numerical method used to solve the problem of pulsating flow in straight, rigid tubes, when the flow waveform is the known quantity, is discussed. As mentioned earlier, the solution for the straight, rigid, tube, with pulsating flow was used to calculate the measured pressured drop across the stenosis, and to evaluate the experimental set-up.

## Method

The governing equation is based on the momentum equation in the axial direction of the pipe. The equation is derived assuming only the axial velocity components  $u(r,t)$  to be non-zero ( $v=w=0$ ), and can be written in dimensionless form as follows:

$$a^2 \frac{\partial u^*}{\partial t^*} = -\frac{\partial p^*}{\partial x^*} + \frac{1}{r^*} \frac{\partial}{\partial r^*} \left[ r^* \frac{\partial u^*}{\partial r^*} \right] \quad (1)$$

with

$$u^* = \frac{u}{\omega R}, \quad r^* = \frac{r}{R}, \quad t^* = t\omega, \quad p^* = \frac{p}{\mu\omega}, \quad x^* = \frac{x}{R} \quad (2)$$

where  $a = R\sqrt{\omega/\nu}$  is the alpha parameter,  $\omega$  and  $\nu$  being the fundamental angular frequency of the pulse and kinematic viscosity of the fluid respectively.

Multiplying Eq. 1 by  $2r^*$  and integrating along the pipe radius, a relation between the time derivative of the flow rate, the pressure gradient, and the wall shear stress can be obtained in the form

$$a^2 \frac{dQ^*}{dt^*} = - \frac{\partial p^*}{\partial x^*} + 2\tau_w^* \quad (3)$$

where  $\tau_w^*$  is the dimensionless shear stress, and  $Q^*$  is the dimensionless volume rate of flow, defined as follows:

$$\tau_w^* = \frac{\tau_w}{\mu\omega} = \left. \frac{\partial u^*}{\partial r^*} \right|_{r^*=1} \quad (4)$$

$$Q^* = \frac{Q}{\pi R^3 \omega} = \frac{1}{0} \int_0^1 u^*(r^*, t^*) r^* dr^* \quad (5)$$

Eliminating the pressure gradient term from Eqs. 1 and 3 and using Eq. 4, the desired differential equation between local instantaneous velocity and flow rate is obtained:

$$a^2 \frac{\partial u^*}{\partial t^*} = a^2 \frac{dQ^*}{dt^*} - 2 \left. \frac{\partial u^*}{\partial r^*} \right|_{r^*=1} + \frac{1}{r^*} \frac{\partial}{\partial r^*} \left[ r^* \frac{\partial u^*}{\partial r^*} \right] \quad (6)$$

To complete the mathematical formulation of the problem, it follows from the axial symmetry of the flow that

$$\frac{\partial u^*(0, t^*)}{\partial r^*} = 0 \quad (7)$$

and from the no-slip condition at the wall

$$u^*(1, t^*) = 0 \quad (8)$$

Finally, assuming a constant velocity distribution over the pipe radius for the time  $t^*=0$ , we arrive at the initial condition

$$u^*(r^*, 0) = Q^* \quad (9)$$

This is selected to satisfy the integral relation (5) for  $t^*=0$ .

The partial parabolic differential Eq. 6, along with the boundary and initial conditions, was solved using a finite difference implicit technique.

#### The Numerical Technique

The grid used was equidistant, that is N equally spaced points along the radius (spatial axis), and NT equally spaced points along the period. Using first order finite difference approximations for the time derivatives, and

second order for the spatial derivatives, the governing Eq. 6 can be written as

$$\begin{aligned}
 a^2 \frac{u_1^{j+1} - u_1^j}{\Delta t} = & a^2 \frac{Q^{j+1} - Q^j}{\Delta t} - 2 \frac{3u_N^{j+1} - 4u_{N-1}^{j+1} + u_{N-2}^{j+1}}{2h} \\
 & + \frac{u_{i+1}^{j+1} - 2u_i^{j+1} + u_{i-1}^{j+1}}{h^2} + \frac{1}{r_i} \frac{u_{i+1}^{j+1} - u_{i-1}^{j+1}}{2h}
 \end{aligned} \tag{10}$$

where:

N denotes point at the wall

h is the spatial step  $1/N-1$

$\Delta t$  is the time step  $2\pi/NT-1$

$r_i = (i-1)h$

The resulting equation is

$$A_i u_{i-1}^{j+1} + B_i u_i^{j+1} + C_i u_{i+1}^{j+1} + E_i u_{N-2}^{j+1} + F_i u_{N-1}^{j+1} + G_i u_N^{j+1} = D_i \tag{11}$$

where:

$$A_i = \Delta t (h - 2r_i)$$

$$B_i = 2r_i (h^2 a^2 + 2\Delta t)$$

$$C_i = -\Delta t (h + 2r_i)$$

$$E_i = 2(\Delta t) h r_i$$

$$F_i = -8(\Delta t) h r_i$$

$$G_i = 6(\Delta t) h r_i$$

$$D_i = h^2 a^2 r_i (v^{j+1} - v^j + u_1^j)$$

The above system of equations can be rewritten in matrix form

$$A_{ik}U_k = D_i \quad (12)$$

where  $A_{ik}$  is a non-symmetric quadratic matrix with elements defined as:

$$\begin{aligned} A_{i,i} &= B_i \\ A_{i,i-1} &= A_i \\ A_{i,i+1} &= C_i \\ A_{i,N-2} &= E_i \quad i = 2, \dots, N-1 \\ A_{i,N-1} &= F_i \\ A_{i,N} &= G_i \end{aligned} \quad (13)$$

The elements of the first row,  $A_{1,k}$ , can be derived from the axial symmetry boundary condition:

$$A_{1,1}=-3, A_{1,2}=4, A_{1,3}=-1, A_{1,4}, \dots, A_{1,N}=0 \text{ and } D_1=0$$

The elements of the last row,  $A_{N,k}$ , can be derived from the no-slip condition at the pipe wall:

$$A_{N,N}=1, A_{N,1}, \dots, A_{N,N-1}=0 \text{ and } D_N=0$$

The system of Eqs. 12 is solved using the Gauss elimination method to give the velocity profiles for the

next instant  $j+1$ . When the end of the period is reached ( $j+1=NT$ ), the calculated velocity profile ( $u_i^{NT}$ ) is substituted to the initial velocity profile ( $u_i^1 = u_i^{NT}$ ) for the next iteration to begin. The procedure continues until the convergence criterion is satisfied.

As mentioned previously, the above numerical solution was used to calculate the pressure drop due to flow in the unobstructed tube,  $\Delta p_f$ , over the distance,  $L$ , between the proximal pressure measuring point, and the distal resistance measuring point (points  $P_1$  and  $P_2$  in Fig. 10). The flow waveform,  $Q(t)$ , was used as the input to the problem. From the solution the velocity profiles  $u(r,t)$  were obtained, and in turn the pressure gradient waveform was calculated, using the expressions (3) and (4). Then, simply by multiplying the pressure gradient waveform by the length,  $L$ , the desired pressure drop over the distance,  $L$ , was obtained.